Chapter 1: Introduction

1.1 General Introduction

Nanotechnology is an arising field of study including the design, manufacturing, characterization and operation of nanoscale patches, materials and systems due to their size-dependent physical and chemical properties (Kandiah *et al.*, 2021). Nano technology is significant for creating new materials, tools and structures because of its

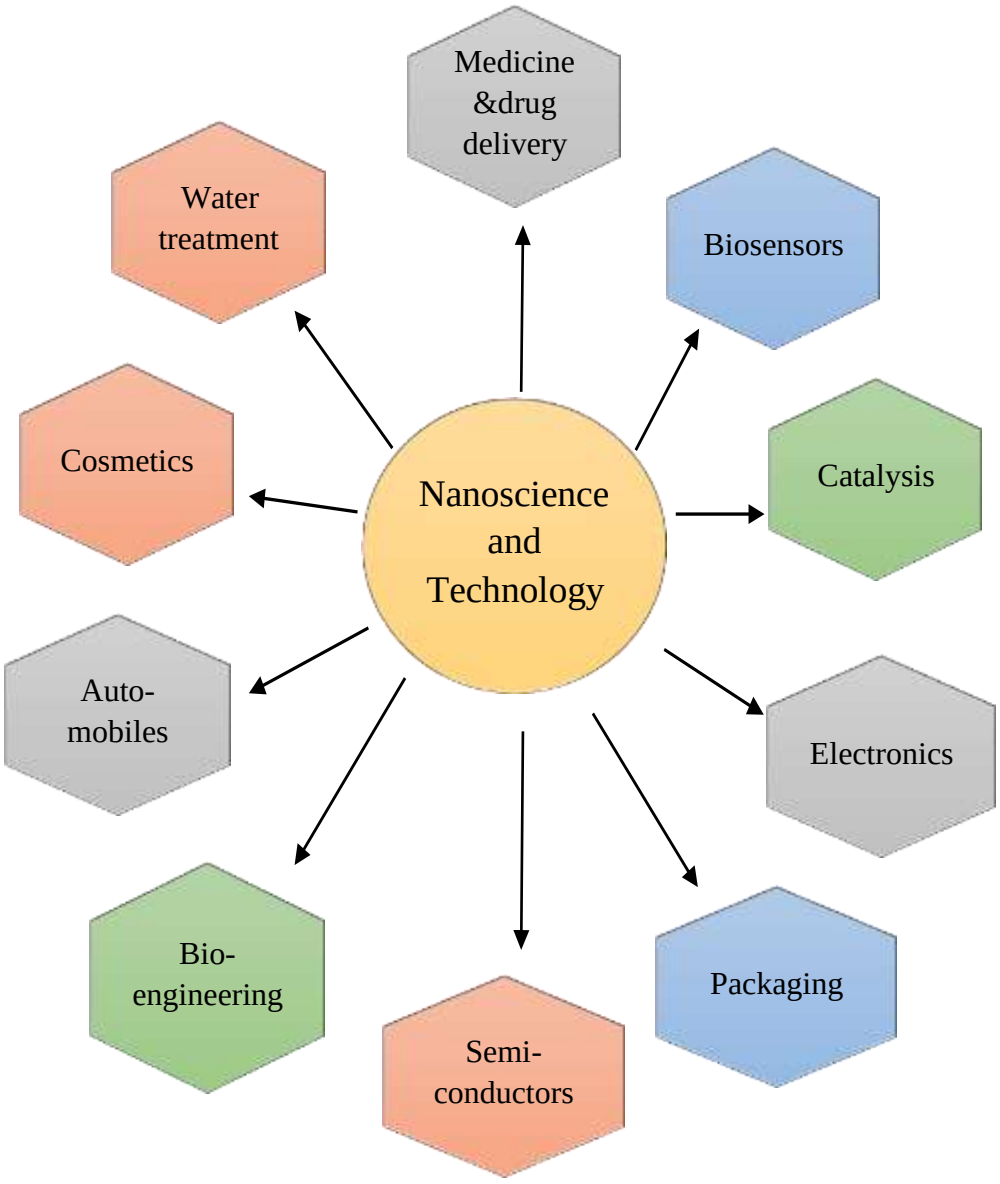

Fig.1.1: Application of nanoscience and technology (Akter *et al.*, 2019)

expertise in understanding, using and controlling matter in confines of a minute scale, analogous to approaching atomic levels (Preetha *et al.*, 2013).

Based on the nanoscale, NPs are microscopic particles having at least one dimension between 1 and 100 nm. NPs contain a very small size and a high surface-to volume ratio, distinguishing their attributes from those of their bulk molecules. NPs are a specifically significant type of nanomaterials having applications in a variety of sectors, (**Fig.1.1**) such as catalysis, electronics, sensing, oil recovery, water treatment, corrosion inhibition, packaging, cosmetics, paint and medication delivery (Akter *et al.*, 2019). As a result of advancement in nanoscience the commercial availability of nanomaterials is expanding; thus, nano-products might be compacted into our daily life. Usually a variety of chemically distinct materials, with metals, metal oxides, polymers, organics, carbon, silicates, non-oxide ceramics and biomolecules are being used for creating NPs. Different morphologies are available of nanoparticles, including cylinders, spheres, platelets, tubes, etc. To satisfy the requirements of the individual applications NPs surfaces are modified for which they are intended. The large variety of NPs, resulting from their wide chemical nature, shapes and morphologies, the medium in which the particles are present, the state of dispersion of the particles and most importantly, the numerous possible surface modifications to which the NPs can be subjected, makes this an effective and efficient area of study (Nagarajan, 2008). There are many different types of dispersion media, including gases (aerosol), liquids, solid matrix and gels for the engineered NPs. As a result of surface modifications, such as DNA grafting, enzyme attachment or surface coatings with nano molecules or charged ligands, nanoparticles characteristics become changed.

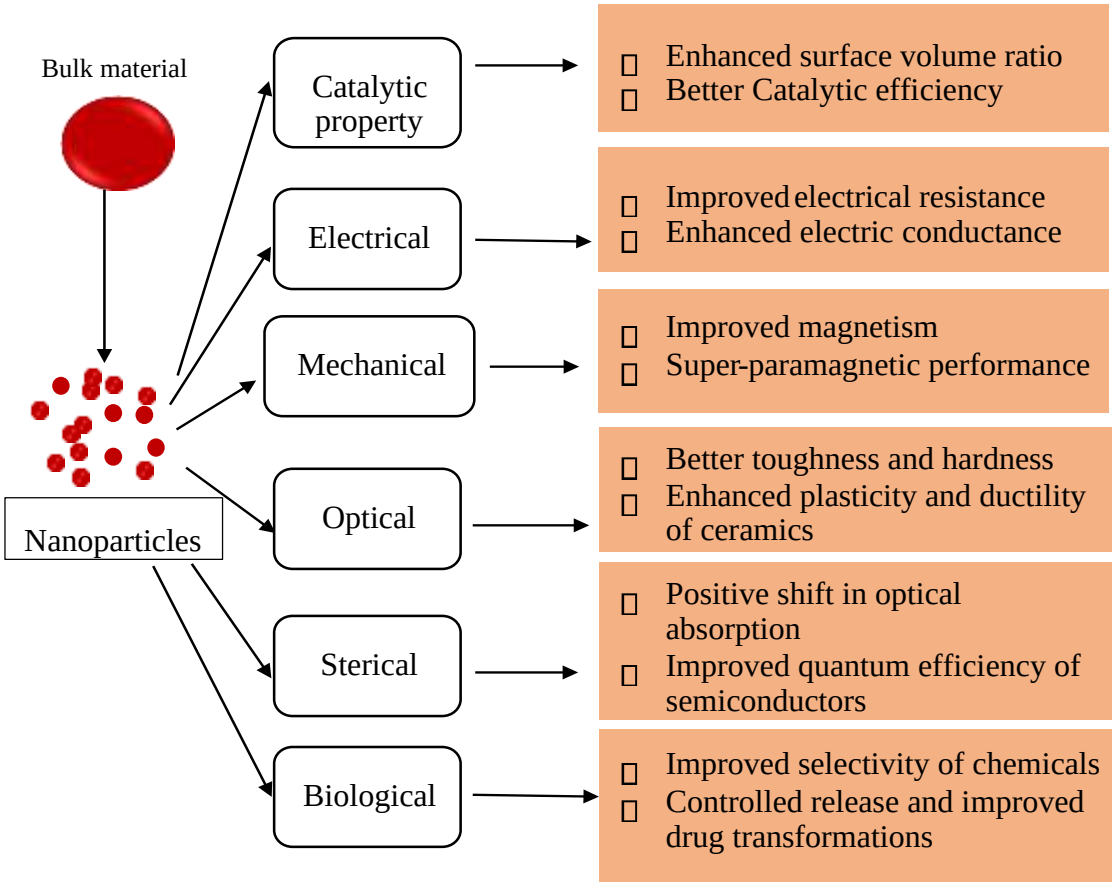

Fig.1.2: Characteristics of nanomaterials

For getting better shape, strength, surface characteristics and catalytic action the NPs are usually tailored. The progress of non-disruptive delivery systems along with nanoscale size, electrical, magnetic, paramagnetic, conductive, photothermal, photoluminescence, dispersing and all other features that can provide therapeutic or diagnostic cures for fatal brain diseases has been made possible by engineering NPs. As fluorescent image probes and MRI agents these designed nanoparticles are employed in biomedical settings. These diverse forms of nanoparticles have efficient properties which make them highly valuable for different types of applications **(Fig. 1.2)**. To create NPs enormous physiological, chemical or biological processes can be used **(Fig. 1.3).**

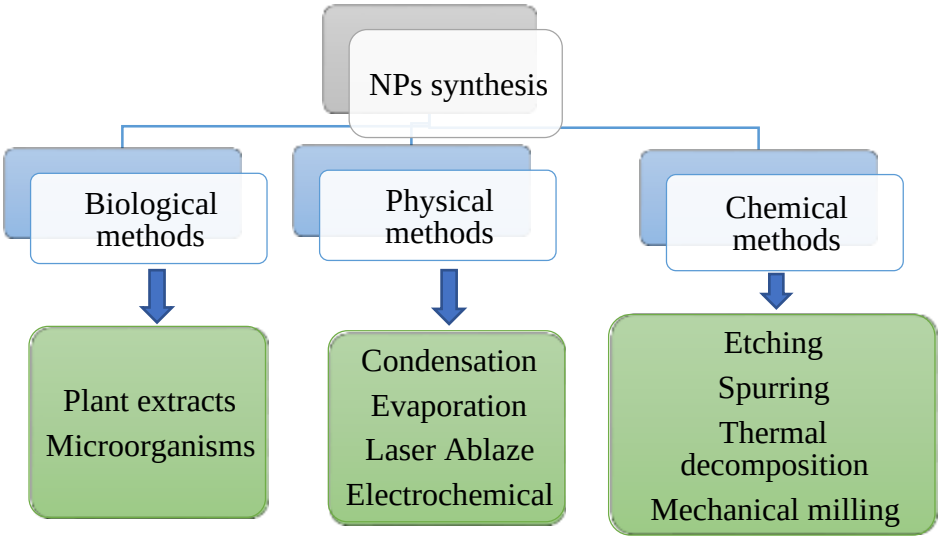

Fig.1.3: Various methods of NP synthesis

Because of having few advantages including low cost, friendly environment, high stability, Calcium carbonate ($CaCO_3$) is getting more attention (Maleki *et al.,2015*). Fabricating porous $CaCO_3$ microspheres (PCMs) has become not only a hot research subject but also a big challenge for researchers in material field. Precipitation, solvothermal and hydrothermal methods using additives such as surfactants, block copolymers, amino acids and so on, these efforts have been done to synthesize PCMs till now. Although these carriers could realize slow-release performance and improve the utilization efficiency of poultry and dairy sector to different degrees, their complicated process and high costs limit their practical applications (Park *et al.,2016).*

As targeted delivery systems the application of nanoparticles (NPs) has attracted considerable attention. Due to its advantages including affordability, low toxicity, biocompatibility, cytocompatibility, pH sensitivity, sedate biodegradability and environment friendly materials $CaCO_3$ has become more familiar (Rabiatul *et al.,2018).*

This research showed that nano calcium can be used as an alternative to commercial calcium carbonate fillers in poultry and dairy industries**.**

1.2 **Aim and Objectives of the Study**

a. To synthesize calcium carbonate nanoparticles by using a suitable method such as precipitation, sol-gel or hydrothermal synthesis

b. To characterize the synthesized nanoparticles by using techniques such as X-ray Diffraction (XRD), Transmission Electron Microscopy (TEM), UV-Visible and Fourier-Transform Infrared (FTIR) Spectroscopy

c. To evaluate the physicochemical properties of the synthesized nanoparticles like particle size, surface area and morphology.

The overall aim of this research project is to provide a safe, effective and sustainable feed additive that can enhance the health and productivity of dairy and poultry animals, leading to higher profitability for farmers and better-quality products for consumers.

Chapter 2: Review of Literature

2.1 Nanomaterials

According to their dimensionality, nanomaterials may take the form of NPs, nanorods, and nanosheets. Nanoparticles are zero-dimensional nanomaterials, nanorods or nanotubes are one-dimensional nanomaterials and two-dimensional nanomaterials are often type one films and layers. These are categorized primarily as isolated NPs. Their physical properties will change, if two or more particles are contacted. Particles containing of these various components are referred as bulk or three-dimensional nanomaterials.

2.2 Types of Nanomaterials

Based on the nanoscale dimensions (<100 nm), they are classified as follows:

- Zero-dimensional nanomaterials (0-D): In this case, all three nanomaterial dimensions are within the nanoscale range. NPs will fall under this category.
- One-dimensional nanomaterial (1-D): Any one dimension will be in the nanoscale range, while the other two dimensions will not. Nanorods, nanotubes and nanowires are under this category.
- Two-dimensional nanomaterials (2-D): Here, any two dimensions are inside the nanoscale range, while the remaining dimension is not. Nanofilms, nanolayers and nano coatings are under this class.
- Three-dimensional or bulk nanomaterials (3-D): In any dimension these NPs are not in nanoscale. They are larger than 100 nm in three arbitrary dimensions, which comprise nanocomposites, core-shell structures, multi-nanolayers, nanowire and nanotube bundles (Kolahalam *et al., 2019*).

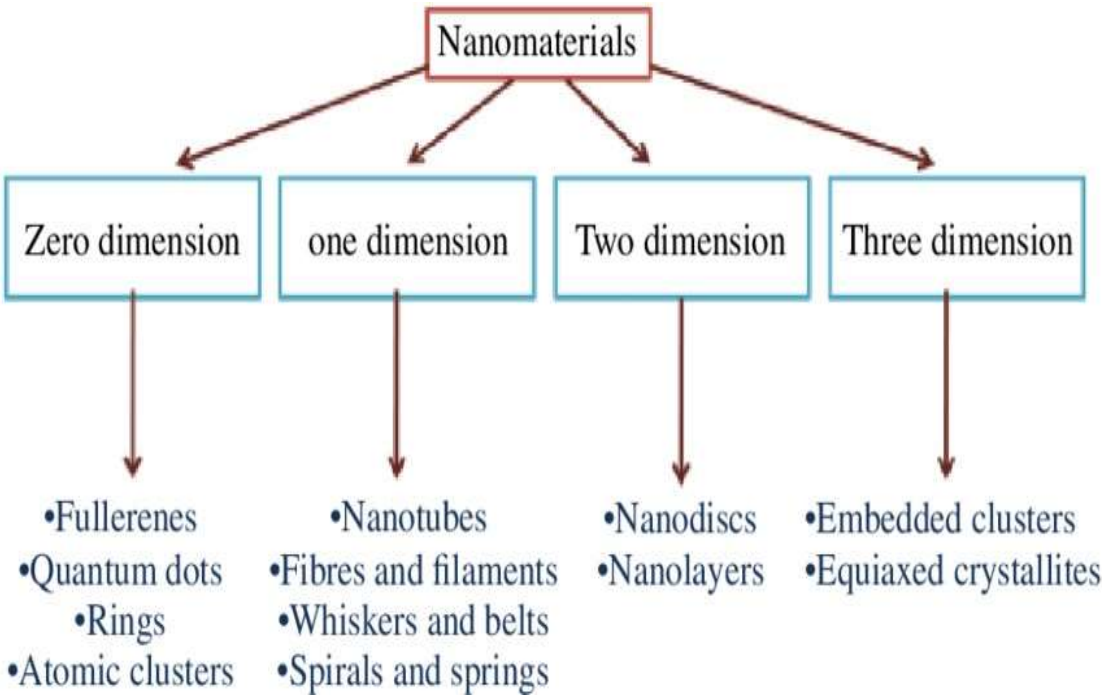

Fig.2.1: Classification of nanomaterials based on dimension

There are various types of nanomaterials present based on their form, size, characteristics and constituents. Based on carbon, metal nanoparticles, semiconductor nanomaterials, polymeric nanomaterials and lipids they are known as nanomaterials.

2. 2.1 Carbon Based Nanomaterials

Primary component of this type of nanomaterial is Carbon. Fullerenes and carbon nanotubes are under this category. CNTs are basically encased in graphene sheets which are coiled into a tube. These are more stronger than steel and easily can be used at reinforce structures. Both single-walled and multi-walled CNTs are exist. Fullerenes are particles consisting by a hollow cage structure with sixty or more carbon atoms. Its structure resembles a football and is made by pentagonal and hexagonal carbon units

structured in a common way. Superior electrical conductivity, electron affinity and tenacity are exhibited by them (Kolahalam *et al., 2019*).

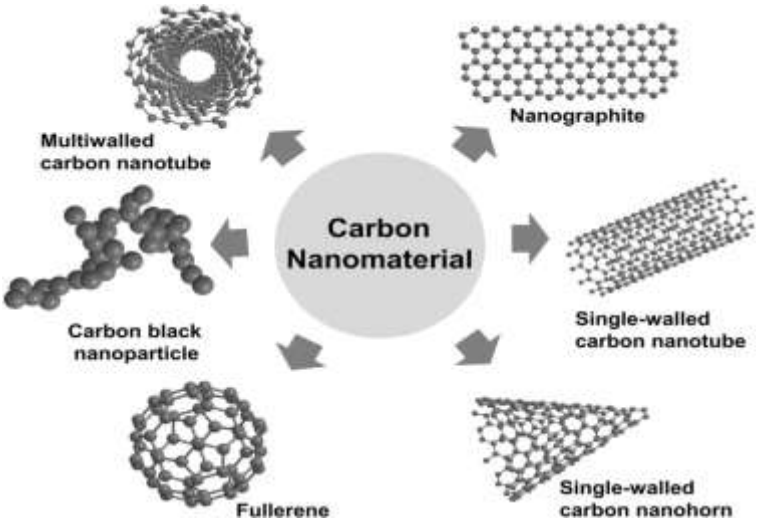

Fig.2.2: Various carbon based nanomaterials (Xuan *et al., 2019*)

2.2.2 Semiconductor Nanomaterials

From semiconductors exhibit metallic and nonmetallic characteristics nanomaterials are derived. For displaying distinct properties large band gaps by modifying the materials are exhibited by them. These are usually employed in photocatalysis and electronic devices. For example, ZnS (Rajabi *et al., 2018*), ZnO (Kolahalam *et al., 2019*). GaN (Aydın, 2018), GaP (Yue *et al., 2006*) and InAs (Lee and McLaurin, 2018) are group III-V elements. In recent years, researchers have been drawn to semiconductor grapheme nanocomposites. Graphene may improve the semiconductor's physical and chemical properties. Materials composited with graphene can be used for gas sensing sensitivity (Sharma *et al., 2009*) and piezoelectric properties (Kolahalam *et al., 2019*).

2.3 Characterization of Nanomaterials

Nanoparticles usually display different physicochemical characteristics. Depending on how big or small, they show various qualities even on the nanoscale. In order to study its properties NPs characterization requires the use of a variety of tools which include the Vibrating Sample Magnetometer, Fourier Transform Infrared (FTIR), Atomic Force Microscopy (AFM), Transmission Electron Microscopy (TEM), Vibrating Sample Magnetometer (VSM), Scanning Electron Microscopy (SEM). Thermogravimetric analysis (TGA), Energy Dispersive X-ray Spectroscopy (EDS), Xray Photoelectron Spectroscopy (XPS), Magnetic Force Microscopy (MFM), Mossbauer Spectroscopy (MS), Electron Paramagnetic Resonance (EPR) and Superconducting Quantum Interference Device (SQUID), (Kolahalam *et al., 2019*).

2.3.1 Determination of Surface Morphology, Surface Area, Size and Shape of NPs

Depend on size and form the primary characteristic of NPs displays distinct physicochemical character. To examine the surface technology AFM, TEM and FESEM can be used. Diameter of NPs can also be calculated. Compositional, morphological and crystallinity information of NPs will be provided by TEM when compared to SEM. HRTEM, FESEM and XRD are three main techniques for calculating nanoparticle sizes. TEM is used normally to determine the size of the NPs (Chekli *et al., 2016*; Gabbasov *et al., 2015*). For determining the size using XRD spectroscopy the Scherrer equation can be used as well in them. Three techniques are useful for calculating the mean particle size and size distribution: Photon Correlation Spectroscopy (PCS), Mossbauer Spectroscopy (MS) and Dynamic Light Scattering

(DLS). To calculate NPs surface area the Brunauer Emmet Teller (BET) method can be used.

2.4 Synthesis of NPs Using Bacteria

Silver, gold bacteria are used as a potent bifactors for synthesizing metal NPs because various inorganic materials extracellular or intracellular are produced by bacteria (Pal *et al., 2019*). Bacteria-mediated AgNPs were first synthesized by the *Pseudomonas Stutzeri* AG259 strain (Haefeli *et al., 1984*). Green synthesis by bacteria is a slow process. AgNPs are biocompatible but some bacteria are resistant to silver.

2.4.1 Synthesis of NPs Using Fungi

As like bacteria fungi show high binding capacity, tolerance, bioaccumulation and ability to take intracellular. Synthesizing nanoparticles by using fungi is easier than others because the growth of fungi is higher than bacteria and easy to control. For the reduction of silver ions into $CaCO_3$ NPs, large amounts of secretion of enzymes such as naphthoquinone, d anthraquinones are responsible (Pal *et al., 2019*).

2.4.2 Synthesis of NPs Using Yeast

Yeast use extracellular proteins to synthesize nanoparticles reported by (Mandal *et al., 2006*). Fungi-mediated fabrication is used to synthesize semiconductors. By using yeast *Candida glabrata, Schizosaccharomyces pombe* various shapes such as monodisperse, spherical, peptide bond, CDs, Quantum crystallites were synthesized (Pal *et al., 2019*).

2.4.3 Synthesis of NPs Using Plants Extract

Plenty of phytochemicals are present in plant part hydrophilic organic compounds are contained in plant materials mainly responsible to reduce ions to Ag (Sathishkumar *et al., 2009*). These are the source of reducing agents, stabilizing agent and capping agent (Bar *et al., 2009,* Rauwel *et al., 2015*). Plant metabolites such as flavonoids, terpenoids, polysaccharides, saponins, alkaloids, organic acid, quinones, amine, alcohol, aldehyde, essential oil and carbohydrates are mainly responsible for the reduction of ions (G. Pal *et al., 2019,* Rafique *et al., 2017*). Green synthesis can be done by using plant extract which involves simply mixing the extract with a solution of the metal precursor at optimized temperature. Synthesis based on plant is faster, easy, cheaper and sustainable synthesis process (Rai *et al., 2008*). Some factors are responsible for characteristics, synthesis rate, the morphology of nanoparticles which are temperature, pH, nature of plant extract, the concentration of precursor, synthesis time etc. (Joy Prabu and Johnson, 2015, Mittal *et al., 2013,* Nakkala *et al., 2016,* P. Singh *et al., 2016*).

2.5 Common methods for producing $CaCO_3$ micro/nanoparticles

Several methods have been designed and used to produce $CaCO_3$ nanoparticles. These methods include:

i. Processing raw $CaCO_3$ sources derived from nature
ii. Carbonation
iii. Solution precipitation
iv. Reverse emulsion and
v. Ultrasound-assisted synthesis.

2.6 General Overview

Due to the potential benefits for animal growth and health nano calcium carbonate ($nCaCO_3$) particles have been increasingly studied as a feed additive in the poultry and dairy industries.

The effects of $nCaCO_3$ on the growth performance, egg quality and mineral deposition of laying hens was investigated in the Journal of Applied Poultry Research (Bashir *et al.,* 2018), It found result as addition of $nCaCO_3$ to the feed improved the egg production rate and eggshell quality including increased the deposition of calcium, phosphorus etc. in the eggshells as well as bones of the hens.

The effects of $nCaCO_3$ on the performance and immune response of dairy cows was evaluated in another study published in the Journal of Dairy Science (Majdoub *et al.,* 2017), the findings showed that milk production becomes increased and immune response of the cows improve due to the addition of $nCaCO_3$ to the diet as evidenced by upper levels of immunoglobulins in their blood.

The potential benefits of $nCaCO_3$ as a feed additive in various animal species was summarized by the authors of the Journal of Animal Science and Biotechnology (Lee *et al.,* 2018), where they showed that $nCaCO_3$ could improve the absorption and utilization of nutrients, enhance growth performance, increase bone mineral density, and reduce the occurrence of diseases in animals. Besides, there are also have few studies that have reported negative effects of $nCaCO_3$ on animal health. For example, a study published in Poultry Science (Majdoub *et al.,* 2016) showed that the addition

of high levels of $nCaCO_3$ to broiler chicken diets decreased their growth performance and caused intestinal inflammation.

Considerable interest as a feed additive in poultry nutrition has gained by Nano calcium carbonate (NCC) and this is happening due to the exceptional physical and chemical properties of NCC, such as high surface area, small particle size and excellent dispersion ability. In a study conducted by (Hassanpour *et al.*, 2016), the effect of NCC on broiler chicken performance was investigated where the results showed that the addition of NCC at a level of 0.5% to the diet significantly improved feed conversion ratio and body weight gain compared to the control group. The researchers concluded that NCC can be considered as a potential feed additive to improve broiler performance.

Another study by (Amerah *et al.*, 2017) investigated the effect of NCC on the growth performance and bone mineralization of broiler chickens and the results showed that the addition of NCC to the diet significantly increased body weight gain and bone mineral density compared to the control group. The researchers revealed that NCC can be utilized as an effective feed additive to improve bone health in broiler chickens.

The effect of NCC on the immune response of broiler chickens was investigated by (Al-Mufarrej *et al.*, 2019). The results showed that the addition of NCC to the diet at a level of 0.5% significantly increased antibody titers against Newcastle disease virus and infectious bronchitis virus compared to the control group. Here the researchers suggested that NCC can be used as an effective immune-modulating agent in broiler chicken nutrition.

Egg production performance and egg quality of laying hens was investigated by (Mahdavi *et al.*, 2019) and the results reported that the addition of NCC to the diet at a level of 0.5% significantly improved egg production and eggshell thickness compared to the control group. The researchers concluded that NCC can be used as an effective feed additive to improve the egg production performance and eggshell quality of laying hens.

Overall, the literatures suggest that NCC can be an effective feed additive in poultry nutrition to improve growth performance, bone health, immune response and egg production performance. However, further research is needed to fully understand the mechanisms of action and optimal dosage levels of NCC in poultry feed.

Chapter 3: Materials and Methods

3.1 Introduction

Four advanced characterization techniques were used in this investigation to investigate the physical and chemical properties of the various $CaCO_3$ powder samples that are produced at laboratory. These techniques included: a) X-Ray diffraction (XRD) spectroscopy, which was used to examine the crystallite size and crystalline structure of the powders b) Fourier transform infrared spectroscopy (FT-IR) that was used to identify functional groups and their respective vibration modes present in the powders c) Electron microscopy *via* Transmission Electron Microscopy (TEM) was used to determine both mean particle size and morphology and d) UV-visible spectroscopy, which was used to investigate the formation of the nanoparticles.

3.2 Study Area

This experiment was carried out in the laboratory of Pulp and Paper Division and Forest Chemistry Division of Bangladesh Forestry Research Institute, Chattogram. Tests were conducted at the departments of Applied Chemistry and Chemical Technology, Chattogram Veterinary and Animal Sciences University (CVASU), Chattogram and Bangladesh Atomic Energy Commission, Dhaka.

3.3 Study Duration

The experiment was conducted for a period of Six months from 10^{th} December, 2022 to 10^{th} June, 2023.

3.4 Collection of Chemicals and Reagents

The chemicals and reagents were collected from the scientific and surgical shop situated at Anderkilla of Chattogram City.

3.5 Required Chemicals and Reagents

In this following study, analytical grade chemicals and reagents were used. The chemicals and reagents that used in this work are listed below:

i. Deionized Water
ii. Calcium Acetate (Loba Chemie Pvt. Ltd., India)
iii. Ammonium Carbonate (BDH Chemicals Ltd, Poole, England)
iv. Soluble Starch (BDH Chemicals Ltd, Poole, England)

3.6 Required Equipment and Instruments

For the synthesis, characterization, formation of the $CaCO_3$ NPs, following equipment and instruments were used:

i. Digital Balance (AY220, Shimadzu Corporation, Japan)
ii. Hotplate Stirrer (JSHS-18D, South Korea)
iii. Centrifuge Machine (DSC-200A-2, Taiwan)
iv. Mortar and Pestle
v. UV-visible Spectrophotometer (1800ENG240V, SOFT, Shimadzu, Japan)
vi. FT-IR Spectrophotometer (Jasco-FTIR-6300, Shimadzu, Japan)
vii. X-ray Diffractometer (Philips, Expert Pro, Netherland)
viii. Transmission Electron Microscope (LEO 1430VP, Netherland)
ix. Vacuum Oven and
x. Desiccator

3.7 Synthesis Procedure of $CaCO_3$ Nano Particles

SS (0.0, 0.25, 0.5g) was added to 100 mL of deionized water under stirring (500 rpm)

Then the resulting solution was heated and kept at 80^0C for 30 min to get a nearly transparent aqueous solution

After cooling to room temperature, CA (1.76 g) was added to the resulting aqueous solution under stirring (500 rpm) for another 30 min at 20, 50 and 80^0C

Afterwards, the AC aqueous solution (0.1 mol/L, 100 mL) was added to the solution

After stirring for 12h, the $CaCO_3$ particles were obtained after centrifugation (10,000 rpm, 5 min) and washed with deionized water three times and drying at 60^0C in a vacuum oven for 12h.

3.8 Characterization of $CaCO_3$ Nano Particles

Characterization of synthesized $CaCO_3$ NPs was performed to determine their physicochemical properties like particle size, surface area and morphology **(Table 3.1)**.

Characterization Techniques	Property Characterized
UV-Vis Spectra Analysis	Formation of Nanoparticles
Fourier Transform Infrared Spectra Analysis (FTIR)	Functional group of organic compounds
Transmission Electron Microscopy (TEM)	Particle size, Surface morphology
X-ray Diffraction Analysis (XRD)	Crystallinity, Particle size

Table 3.1: Characterization techniques of synthesized $CaCO_3$ NPs

3.8.1 UV-Vis Spectroscopy

The reduction of pure $CaCO_3$ was observed by measuring the UV-Vis spectra of the reduction media by using a 3 ml sample and comparing it to a 3 ml blank of distilled water. To record the UV-Vis spectra of the resultant colloidal solution of the expected $CaCO_3$ NPs in the wavelength region of 185-800nm, a UV-Vis spectrophotometer was used. The baseline was adjusted by using distilled water as a reference blank (Shafaghat, 2015; Uddin *et al.,* 2020).

Fig 3.1. UV-vis Spectroscopy

3.8.2 Fourier Transform Infrared (FT-IR) Analysis

FT-IR spectroscopy investigation on the $CaCO_3$ powder samples since the FT-IR spectrum can help to distinguish between the different phases of calcium carbonate crystals. All crystal phases can be discriminated by detecting and identifying the absorption bands because each phase of $CaCO_3$ has some characteristic absorption bands. Fourier transform infrared spectroscopy (FT-IR) was used basically to identify the presence of intrinsic functional groups in $CaCO_3$ NPs from the biomolecules present in the powder of $CaCO_3$. To record IR spectra in the mid-IR band (4000-400 cm^{-1}), FT-IR spectrophotometer (Jasco-FTIR-6300, Japan) was used. In order to get IR spectra dry and solid $CaCO_3$ NPs (1% w/w) powder was homogeneously combined with pure and dry KBr powder in a quartz mortar using a pestle and then compressed mechanically under a pressure of 8-10 tons in a metal holder to form a translucent pellet. The pellet was then placed in the direction of the instrument's IR beam with a sample holder to get the spectral measurement. The baseline of the spectrum was modified using KBr after getting spectra of the material (Preetha *et al.,* 2013).

Figure 3.2. FT-IR/ NIR Spectrometer Chemical composition

3.8.3 Transmission Electron Microscopy (TEM)

Electron microscopy was pioneered in the late nineteen-thirties by Manfred von Ardennes and Helmut Ruska. But extensive scanning electron microscopy development only started in the early nineteen fifties and unlike conventional optical microscopy, Transmission electron microscopy (TEM) uses electrons as a substitute for light emission to an image sample. The TEM operates by using a vacuum and with the help of electron guns, the source of electrons are produced at the top of the microscope. The electrons travel vertically downwards towards the sample holder. Electromagnets control their passage which produce electromagnetic fields that act as lenses to guide and focus the electron beam. Both electrons and X-rays are ejected from the sample when the beam once strikes the sample. To generate a high-resolution digital image of the sample, in the lower part of the microscope, detectors gather the X-rays, backscattered electrons and secondary electrons and finally convert them into a signal (Riehemann *et al*., 2009).

There are several advantages present in TEM technique, such as a considerable depth of area and a high degree of magnification that can handle various samples. Additionally, TEM also generates qualitative elemental compositional analysis,

quantitative analysis, x-ray line scans and mapping. These advantageous features enable the TEM technique to study microstructures and material defects like fractures, corrosion particle size and morphology and grain size determinations and boundaries. However, before imaging in the TEM, non-conductive samples need to be coated (gold, carbon and platinum) to promote conductivity (Prasad *et al*., 2012).

To investigate the size and morphology and elemental composition of the respective $CaCO_3$ micro/nano powder samples, electron microscopy studies were undertaken. A thin sample layer was put on a carbon-coated copper grid (Kabir *et al.*, 2020).

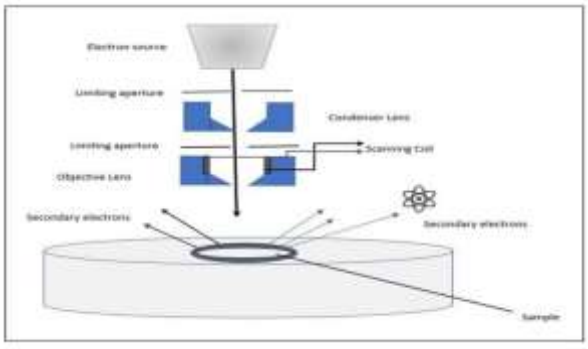

Figure 3.3. Operating principle of the TEM

Figure 3.4. TEM, LEO 1430VP Neo-Scope TM electron microscope

3.8.4 X-ray Diffraction (XRD) Analysis

Analysis of $CaCO_3$ NPs through X-ray diffraction (XRD) were performed by X-ray Diffractometer (Philips, Expert Pro, Netherland). The powder samples were placed in a square aluminum sample holder (40mm × 40mm) with a 1mm deep rectangular hole (20mm × 15mm) and placed against an optical smooth glass plate. With the help of sample holder the upper surface of the sample was labeled in the plate. The sample holder was then placed in the diffractometer to get the diffraction pattern (Anandalakshmi *et al*., 2019).

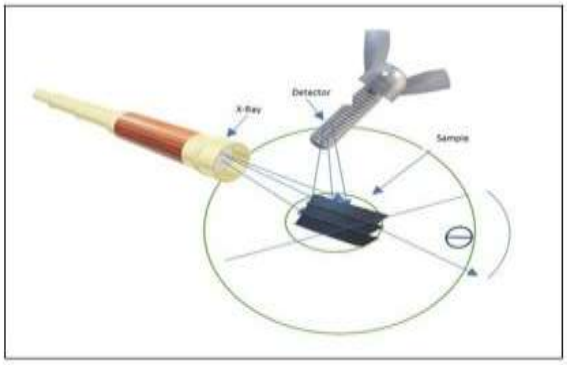

Figure 3.5. Schematic of three main components of an XRD

Figure 3.6. X-ray powder diffractometer for $CaCO_3$ analysis

3.9 Statistical Analysis

“Originpro”, “Image software” and “Excel software” were used during the graphical presentation and data analysis.

Chapter 4: Result

4.1 UV-Vis Spectroscopy

The synthesized CCNPs were initially characterized by UV-Vis Spectroscopy. **Figures (4.1-4.4)** display the UV-Vis spectra of CCNPs in the wavelength range of 185 to 800 nm at different temperature (Ghadami *et al., 2013*). Calcium carbonate nano powders were partially dissolved in deionized water through vortex mixer to obtain the UV absorption bands. The strong absorbance value obtained for calcium carbonate nanoparticles in the range of 200 to 300 nm in UV that indicates the formation of CCNPs in the samples (Diningsih and Rohmawati, 2022). In the figures, the UV absorption spectrum of CCNPs showed the strong absorbance value of 2.742 (sample A at 20^0 C), 2.775(sample B at 50^0 C), 2.692 (sample C at 80^0 C) in the wavelength of 205nm, 216nm and 209 nm respectively. So, the UV analysis confirms the presence of CCNPS in the samples.

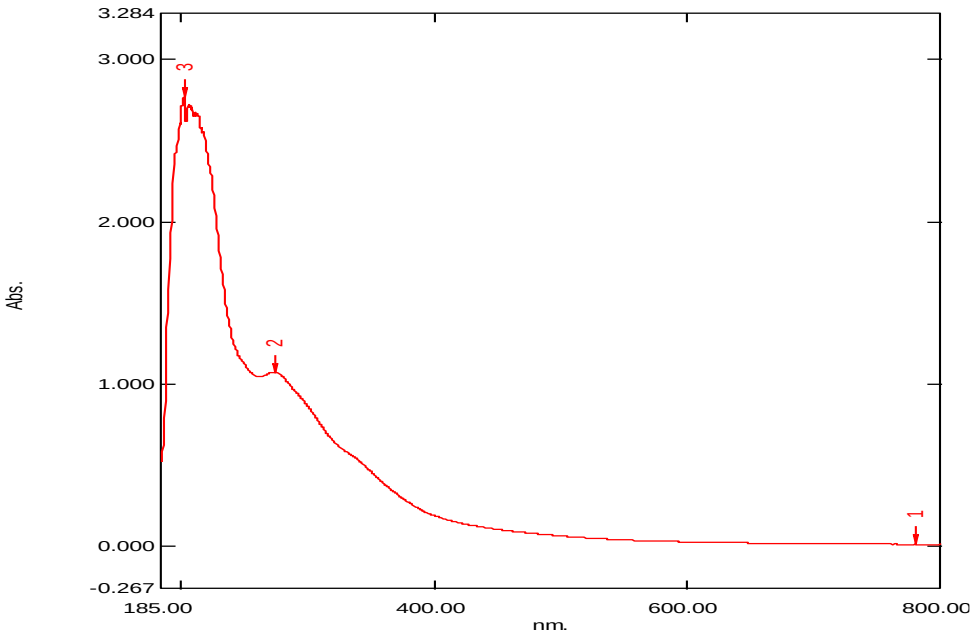

Fig. 4.1: UV-vis spectra of synthesized $CaCO_3$ nanoparticles at 20^0 C

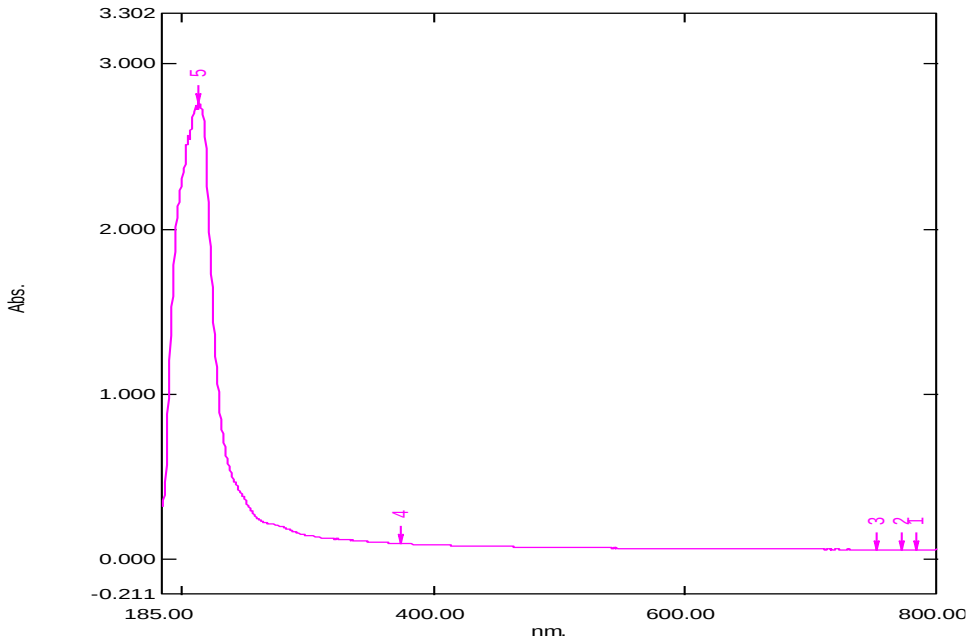

Fig. 4.2: UV-vis spectra of synthesized $CaCO_3$ nanoparticles at 50^0 C

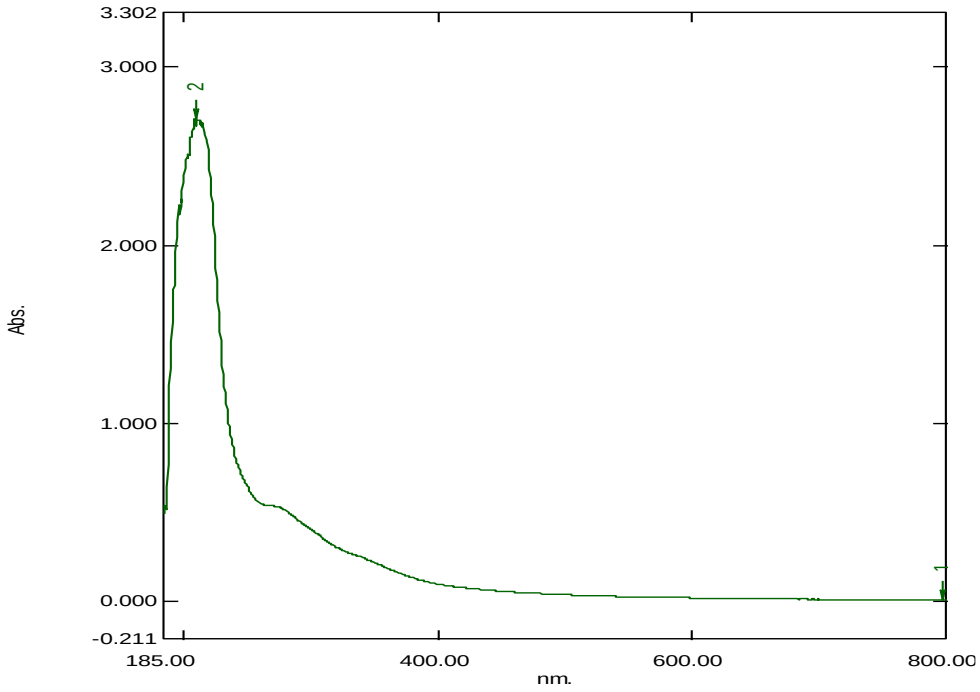

Fig. 4.3: UV-vis spectra of synthesized $CaCO_3$ nanoparticles at 80^0 C

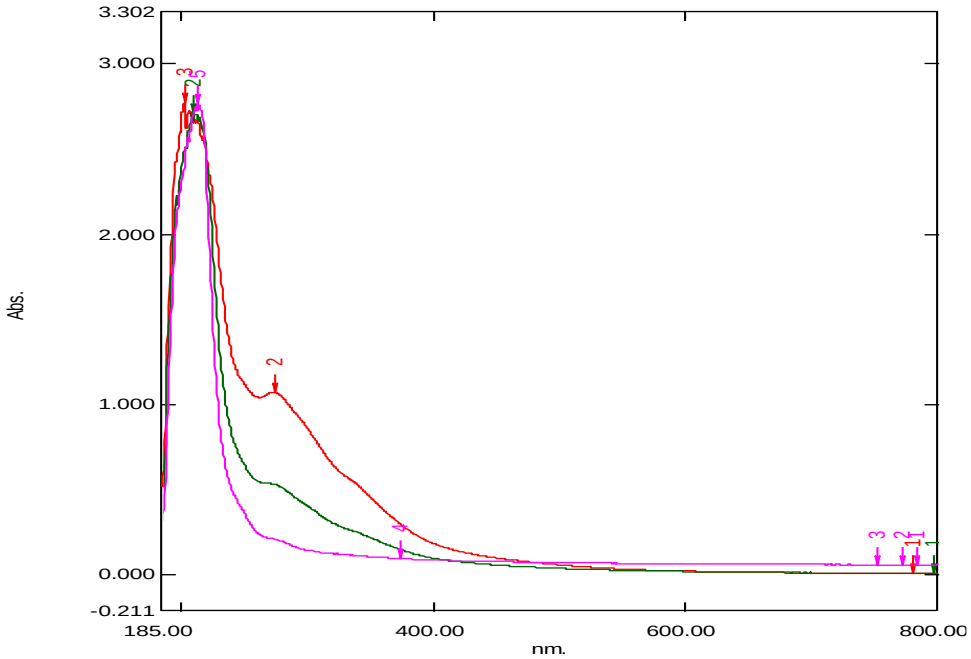

Fig. 4.4: Combined UV-vis spectra of synthesized $CaCO_3$ nanoparticles at 20^0 C, 50^0 C and 80^0 C

4.2 Fourier Transform Infrared Spectroscopy (FT-IR)

To identify the functional groups and chemical bonds FT-IR analysis are usually used. FT-IR spectra of synthesized nanoparticles exhibiting the functional groups and chemical bonds on the surface of nanoparticles are showed at **Figures (4.5-4.8)** and display that FT-IR spectrum was generated by the absorption of electromagnetic radiation in the frequency range 500-4000cm-^{1}. The molecular structure of $CaCO_3$ with associated functional groups is revealed through the appearance of several peaks. The spectrum showed the vibrational bands at 1400cm-^{1},1100cm-^{1}, 1200cm-^{1}, 875cm-^{1} and 750cm-^{1} are described to the asymmetric stretching, symmetric stretching, out-of-plane bending, in-plane bending vibrations of carbonate respectively that indicates the presence of carbonate (Wang *et al.,* 2018). It is confirmed by FT-IR analysis that the calcium carbonate nanoparticles have the characteristic peak of carbonate group. The

peaks confirmed that the nanoparticles could be possible of calcite phase. Furthermore, the IR spectrum of $CaCO_3$ nanoparticles represents peaks at 518cm-^{1}, 588.12cm-^{1}, 814cm-^{1}, 1142.30cm-^{1} respectively corresponding to the Ca-O, O-H, C-H and C-C vibrations. The peaks at 3000cm-^{1} and 1600 cm-^{1} assigned to the stretching and bending vibrations of -OH of SS. It is also evidenced that the calcium carbonate nanoparticles consisted of $CaCO_3$ itself (Xiang *et al.,* 2018).

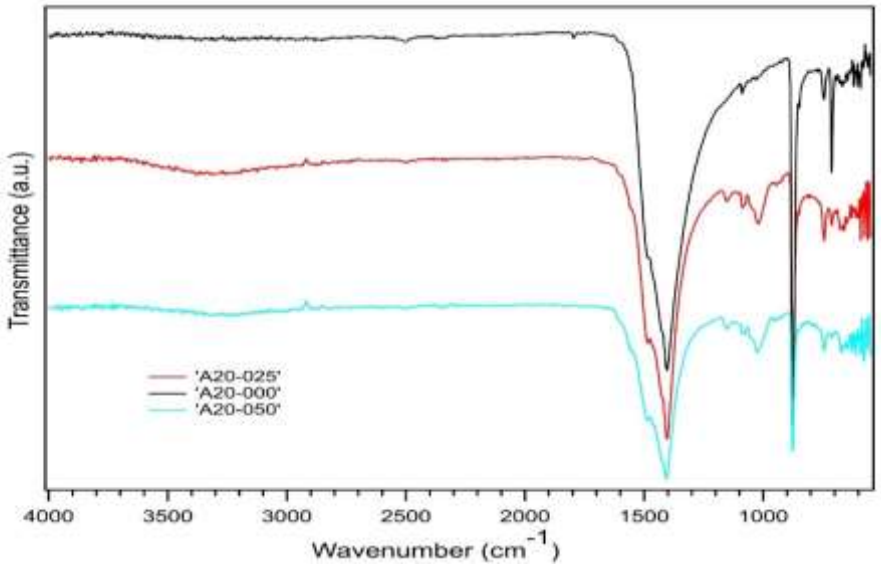

Fig.4.5: FTIR spectra of synthesized $CaCO_3$ nanoparticles at 0.0 gm, 0.25gm, 0.50gm of Starch concentration at 20^0 C

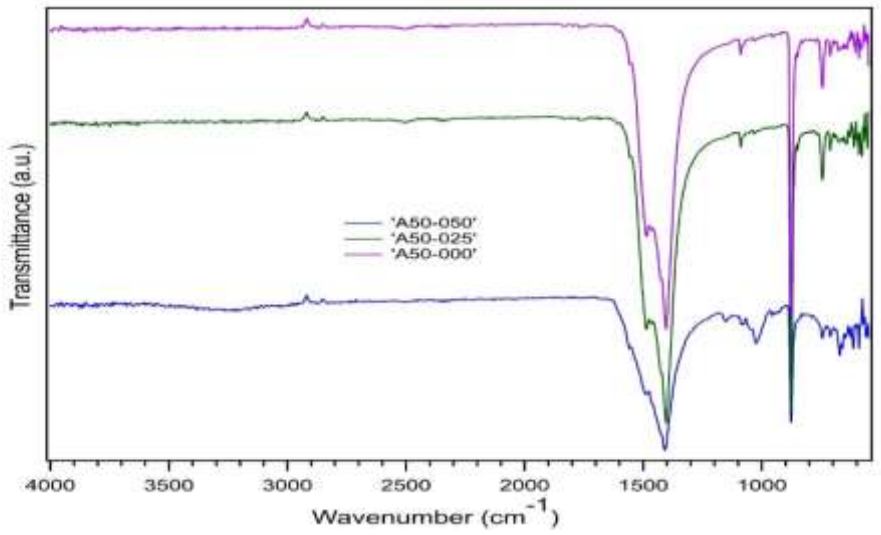

Fig.4.6: FTIR spectra of synthesized $CaCO_3$ nanoparticles at 0.0 gm, 0.25gm, 0.50gm of Starch concentration at 50^0 C

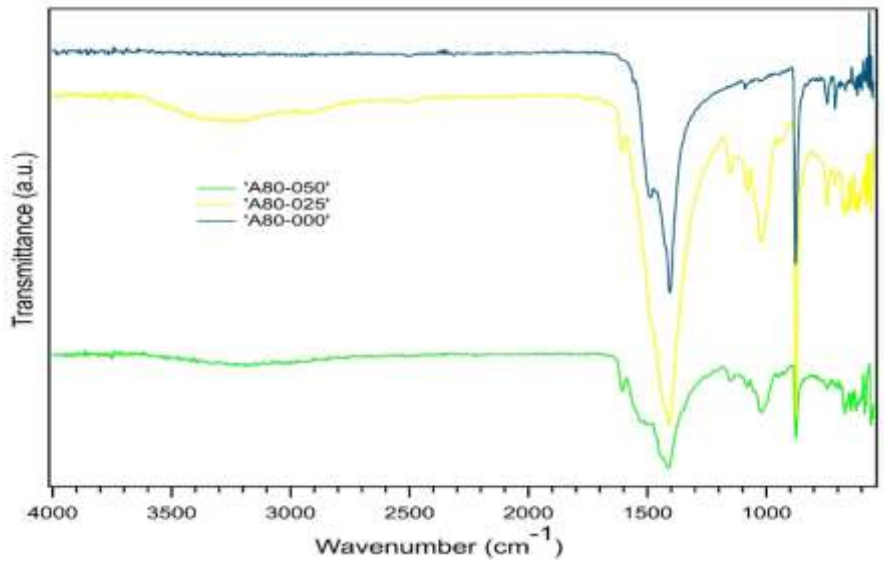

Fig.4.7: FTIR spectra of synthesized $CaCO_3$ nanoparticles at 0.0 gm, 0.25gm, 0.50gm of Starch concentration at 80^0 C

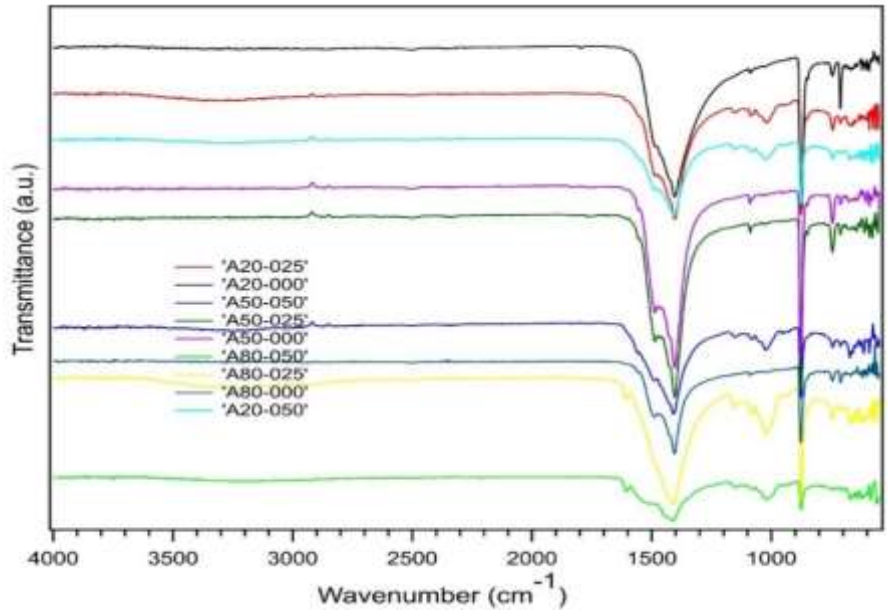

Fig.4.8: Combined FTIR spectra of synthesized $CaCO_3$ nanoparticles at 0.0 gm, 0.25gm, 0.50gm of Starch concentration at 20^0 C, 50^0 C and 80^0 C

4.3 X-ray Diffraction (XRD)

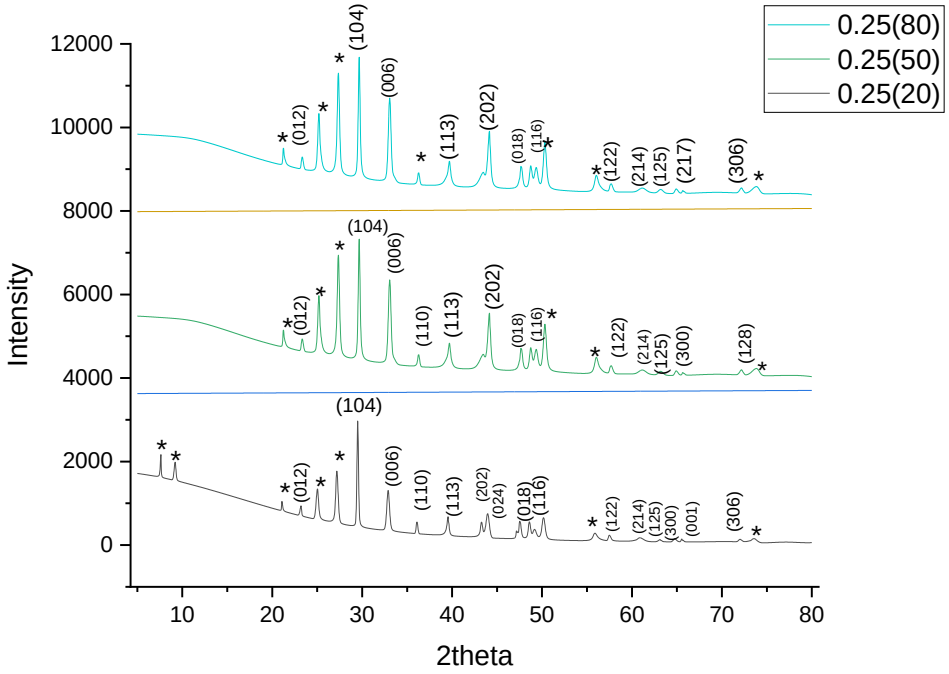

Fig.4.9: Peak positions for synthesized $CaCO_3$ nanoparticles in XRD analysis (The asterisk marks denote unassigned peaks)

The crystal structure and phase identification of the CCNPs samples were analyzed using the X-ray diffraction pattern. The XRD spectra were recorded and observed 2θ, h k l values with a diffraction angle between 20° to 80° for all the CCNPs sample at 20°C, 50°C, 80°C. The crystallite size was determined from the broadenings of the corresponding X-ray spectral peaks by using Scherrer's formula. The average nano-crystalline size(D) was calculated using the Scherrer formula (Shivaraj *et al.,* 2017).

$$D = \frac{K\lambda}{\beta \cos\theta}$$

Where, λ is the wavelength of X-ray radiation source (0.15406), k is the geometric factor (0.9), β is the FWHM (full-width at half maximum) of the XRD peak at the diffraction angle θ.

Plane (h k l)	Peak Position 2θ(degree)	FWHM (degree)	Crystallite Size, D(nm)	Average Crystallite Size(nm)
0 1 2	23.21	0.18	45.8	40.65
1 0 4	29.49	0.17	48.0	
0 0 6	31.45	0.33	26.0	
1 1 0	36.07	0.19	46.6	
1 1 3	39.55	0.22	41.0	
2 0 2	43.23	0.21	42.1	
0 2 4	47.15	0.13	68.5	
0 1 8	47.50	0.21	42.7	
1 1 6	48.55	0.24	38.5	
1 2 2	57.46	0.24	39.7	
2 1 4	60.76	0.77	12.5	
1 2 5	63.13	0.30	33.0	
3 0 0	64.73	0.33	29.6	
0 0 1	65.53	0.15	64.6	
3 0 6	73.45	0.63	16.5	

Table 4.1: Structural parameters of synthesized CCNPs from the XRD analysis at 20°C

As shown in **Figure 4.9** illustrates the **Table 4.1** displays the result of the XRD analysis show that each diffraction peak is at an angle of 23.21°, 29.49°, 36.07°, 39.55°, 43.23°, 47.15°, 47.50°, 48.55°,57.46°, 60.76°, 63.13°, 64.73°, 65.53° and 73.45° with Miller index (012), (104), (006), (110), (113), (202), (024), (018), (116), (122), (214), (125), (300), (001) and (306) indicates the crystallographic planes of calcite respectively in the CCNPs sample at 20°C (Luo *et al.,*2020). The diffraction peak data on the synthesis results are the following JCPDS PDF number (01-080-9776). Calculated crystalline

size of the CCNPs (20°C) were found within the range of 11nm to 70 nm with an average of 40.65 nm.

Plane (h k l)	Peak Position 2θ (degree)	FWHM (degree)	Crystallite Size, D(nm)	Average Crystallite Size(nm)
0 1 2	23.31	0.25	34.2	26.58
1 0 4	29.66	0.21	40.3	
0 0 6	31.58	0.33	26.5	
1 1 0	36.24	0.22	39.0	
1 1 3	39.68	0.35	25.6	
2 0 2	43.44	0.71	12.5	
0 1 8	47.64	0.25	36.4	
1 1 6	48.72	0.29	31.0	
1 2 2	57.59	0.33	28.9	
2 1 4	61.10	0.91	10.6	
1 2 5	63.14	0.56	17.4	
3 0 0	64.89	0.31	31.3	
1 2 8	73.82	0.88	11.8	

Table 4.2: Structural parameters of synthesized CCNPs from the XRD analysis at 50°C

As shown in **Figure 4.9** illustrates the **Table 4.2** that the peaks with diffraction angle were observed at 23.31°, 29.66°, 36.24°, 39.68°, 43.44°, 47.64°, 48.72°, 57.59°, 61.10°, 63.14°, 64.89°and 73.82° which corresponds to the lattice planes (012), (104), (006), (110), (113), (202), (018), (116), (122), (214), (125), (300) and (128) respectively. This data is in good agreement with the JCPDS card no. (01-080-9776) which proves that $CaCO_3$ NPs is existed in calcite form (Kadota *et al.,* 2020). The particle size of the

nanoparticles estimated by the relative intensity of peaks and peak sharpness found within the range of 11nm to 40 nm with an average of 26.58 nm.

Plane (h k l)	Peak Position 2θ (degree)	FWHM (degree)	Crystallite Size, D (nm)	Average Crystallite Size(nm)
0 1 2	23.01	0.32	26.5	32
1 0 4	29.33	0.26	33.1	
0 0 6	31.35	0.39	22.2	
1 1 3	39.38	0.37	24.0	
2 0 2	43.15	0.12	71.7	
0 1 8	47.42	0.21	43.6	
1 1 6	48.45	0.20	46.4	
1 2 2	57.39	0.18	53.0	
2 1 4	60.27	4.10	2.30	
1 2 5	62.92	0.42	23.2	
2 1 7	68.68	0.98	10.2	
3 0 6	73.45	0.57	18.1	

Table 4.3: Structural parameters of synthesized CCNPs from the XRD analysis at 80°C

As shown in **Figure 4.9** illustrates the **Table 4.3** that the XRD patterns of the synthesized CCNPs at 80°C obtained peaks at 2θ° values of 23.01°, 29.33°, 39.38°, 43.15°, 47.42°**,** 48.45°**,** 57.39°**,** 60.27°**,** 62.92°**,** 68.68° and 73.45° corresponding to the planes (012), (104), (006), (113), (202), (018), (116), (122), (214), (125), (217) and (306) respectively demonstrating the structure of $CaCO_3$ phases with the JCPDS card no.(01-080-9776). The presence of sharp peaks denotes the highly crystalline $CaCO_3$ in the sample (Mensah *et al.,* 2022). The crystal size of the synthesized CCNPs were estimated about 10nm to 72 nm with an average of 32 nm.

4.4 Transmission Electron Microscopy (TEM)

The morphology of synthesized CCNPs at various temperature was determined by using TEM analysis. **Figures (4.10-4.12)** show the TEM micrographs of synthesized CCNPs at various magnifications and provide details on their surface morphology, size and shape distribution (Xue *et al.,* 2015).

The synthesized CCNPs displayed their average particle size, average particle length and average aspect ratio in a histogram during the TEM investigation. At 20°C, the typical CCNPs particle size, length and aspect ratio are 44 ± 10 nm, 148 ± 37 nm and 3.36 respectively. The synthesized CCNPs have an average particle size, length and aspect ratio of 29 ± 4 nm,84 ± 13 nm and 2.90 at 50°C.The average particle size, length and aspect ratio of the synthesized CCNPs at 80°C are in that order,105 ± 65 nm, 189 ± 167 nm and 1.80. Therefore, the TEM images confirm that the CCNPs nanoparticles were properly crystallized and had a rod like structure (Atta *et al.,* 2016).

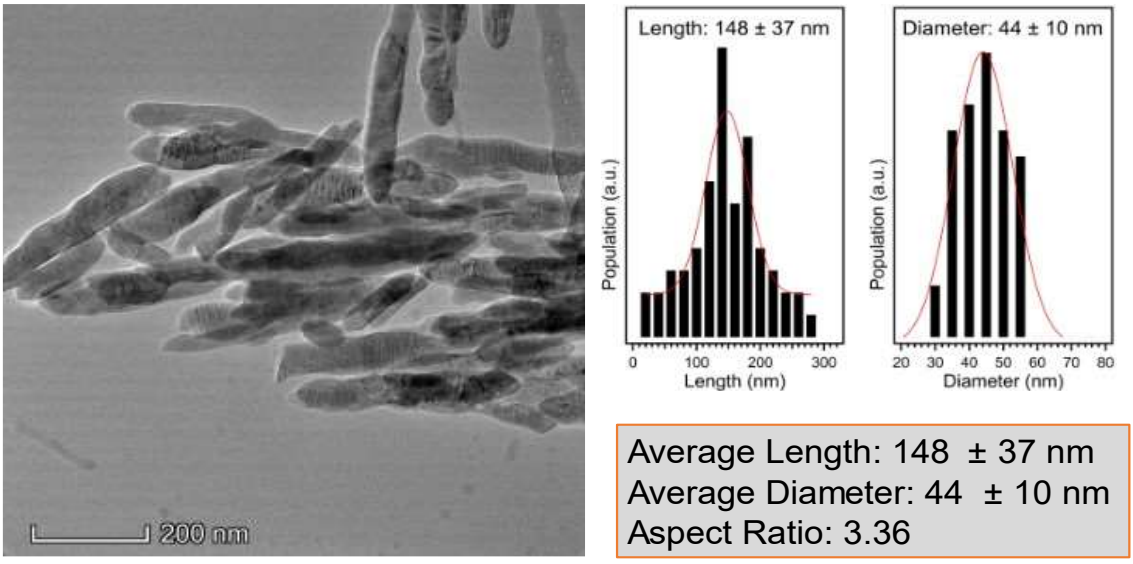

Fig.4.10: TEM image, Particle length distribution and Particle size distribution of CCNPs at 20^0C

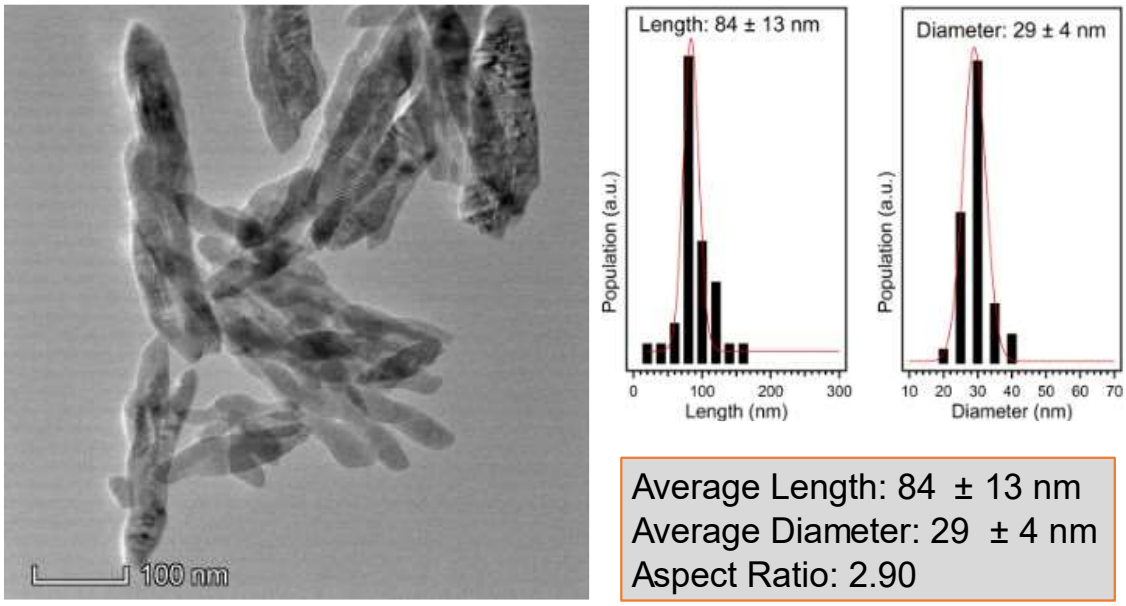

Fig.4.11: TEM image, Particle length distribution and Particle size distribution of CCNPs at 50^0C

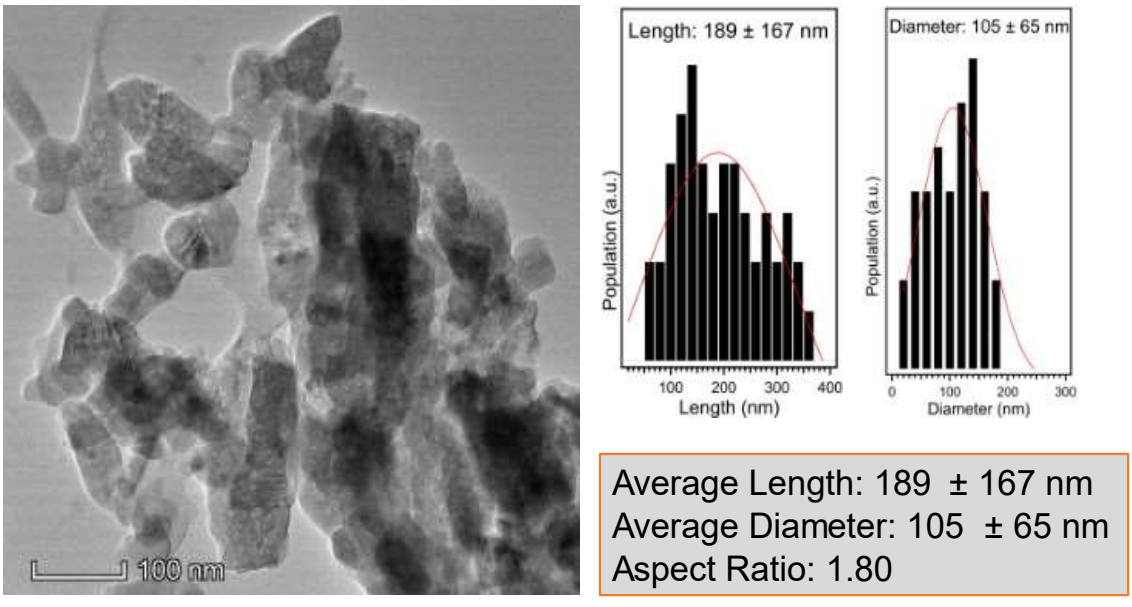

Fig.4.12: TEM image, Particle length distribution and Particle size distribution of CCNPs at 80^0C

Chapter 5: Discussion

5.1 UV-Vis Spectroscopy Analysis

The technique of UV-vis spectroscopy is employed to identify the existence of calcium carbonate nanoparticles in a sample. In UV Spectrophotometer, the absorbance value obtained for calcium carbonate nanoparticles sample in the range of 200 nm to 300 nm that produces strong absorbance peak confirming the formation of CCNPs in the sample (Diningsih and Rohmawati, 2022).

Figures (4.1-4.4) display the UV absorption spectrum found in the different wavelength along with absorbance value in CCNPs sample. At 20°C, the sample showed the different absorbance value of 2.742, 1.073, 0.011 in the range of 205 nm, 272 nm and 728 nm suggesting the presence of calcium carbonate nanoparticles (Shivaraj *et al.,*2017). The absorption peak observed at 211 nm ,216 nm, 357 nm and 763 nm along with the absorbance value of 2.755, 2.775, 0.084, 0.045 in the CCNPs sample at 50°C that reporting the presence of calcium carbonate (Gupta *et al.,* 2015). The UV spectrum of another sample (at 80°C) revealed the absorption rate of 0.009, 2.692 at 209 nm and 780 nm (Hariharan *et al.*, 2014).

Among the three sample, the CCNPs sample (50°C) showed the greater absorbance value in the UV absorption spectrum. So, the strong absorbance peak obtained for CCNPs sample in the range of 216 nm. By capturing the UV-Visible spectra of a solution containing CCNPs, the formation of CCNPs was further validated.

5.2 Fourier Transform Infrared Spectroscopy (FT-IR) Analysis

Fourier transform infrared spectroscopy (FT-IR) is used to identify functional groups and their respective vibration modes present in the calcium carbonate nanoparticles. The different phases of calcium carbonate crystals can be distinguished by FT-IR

spectrum. By detecting and identifying the absorption bands all $CaCO_3$ crystal phases can be discriminated. The absorption bands of a carbonate-based material have normal modes of vibration peaks: a) Symmetric stretching at about 1080 cm^{-1} (ν1); b) The out-of-plane bending absorption at about 870 cm^{-1} (ν2); c) Asymmetric stretching at about 1400 cm^{-1} (ν3) and d) In-plane bending around 700 cm^{-1} (ν4) (Nasseh, 2021). The graphs displayed that FT-IR spectrum was generated by the absorption of electromagnetic radiation in the frequency range 500-4000cm^{-1}. The spectrum showed vibrational bands at 1400 cm^{-1}, 1100 cm^{-1}, 1200 cm^{-1}, 875 cm^{-1} and 750 cm^{-1} are described to the asymmetric stretching (v3), symmetric stretching (v1), out-of-plane bending (v2), in-plane bending vibrations (v4) of carbonate respectively that indicates the presence of carbonate (Wang *et al.,*2018). It is ensured that the calcium carbonate nanoparticles had the characteristic peak of carbonate group. The stretching and bending vibrations of -OH of SS is assigned to the peaks at 3000 and 1600 cm^{-1}. Besides, the FTIR peak of SS at 1155 cm^{-1} described to the C-O stretching vibration of the -C-O-H group and the other peak at 1080 cm^{-1} was corresponding to the O-C stretching vibration. The antisymmetric stretching vibration of C-O is assigned to the peak at 1540 cm^{-1} and the twisting and stretching vibrations of O-C-O appeared in the FTIR spectrum of SS-CA are corresponded to the peaks of 676 and 612 cm^{-1}, which indicates the incorporation of CH_3COO- with SS. The intensity of the peak at 3370 cm^{-1} decreased distinctly when SS bond CA and the peak at 1644 cm^{-1} shifted to 1614 cm^{-1}, indicating the formation of hydrogen bonds between the -COOH of AC and -OH of SS, which was favorable for adsorbing Ca^{2+} in the SS aggregate. The peak at 1022 cm^{-1} corresponding to the C-OH stretching vibration of SS likely attributed to the chelation of Ca^{2+} by the -OH of SS (Xiang *et al.,* 2018). Furthermore, the IR spectrum

of $CaCO_3$ nanoparticles represents peaks at 588.12cm-^{1}, 814cm-^{1} and 1142.30cm-^{1} respectively corresponding to the O-H, C-H and C-C vibrations (Kazemi *et al.,* 2021).

5.3 X-ray Diffraction (XRD) Analysis

X-ray powder diffraction (XRD) analysis was performed to monitor the crystallographic structure of the CCNPs in the sample at 20°C, 50°C and 80°C. The diffraction patterns of CCNPs showed characteristic peaks which indicate the crystallinity of the synthesized calcium carbonate nanoparticles. A dominant phase of calcite was observed evidenced although a trace of vaterite was also seen in the CCNPs sample. The broad diffraction peaks indicate that calcite and vaterite were the principal crystalline polymorphs corresponding respectively to (h k l) namely (012), (104), (110), (113), (018), (116), (125), (300), (110), (116), (214) and (300) (Ali Said *et al.,* 2020).

A recent study of XRD pattern of the CCNPs investigated that the obtained peaks at 2θ° values of approximately 23°, 29.4°, 36°, 39.4°, 43.1°, 47.5°, 48.5°, 57.5° and 65° corresponding to the planes of (012), (104), (006), (110), (113), (202), (018), (116), (122), (300) suggesting the presence of crystalline calcite in the sample (Kadota *et al.*, 2020).

In this study, all CCNPs sample exhibit the same highest diffraction peak at 2θ°=29.5° in the planes of (104) at different temperature. The average particle size of nanoparticles found to be 40.65 nm, 26.58nm, 32nm as estimated by Scherrer formula that indicates that particles are in crystalline structure (Dehghani *et al.,* 2019, Biradar *et al.,* 2011). At 50°C, the calculated average crystallite particle size found to be the smallest compared to other two samples. In XRD analysis, the lattice parameter of all CCNPs sample at different temperature also prove that they are in hexagonal crystalline structure.

5.4 Transmission Electron Microscopy (TEM)

The morphological structure, particle size, shape, and distribution of the CCNPs in the sample at 20°C, 50°C and 80°C were all examined by using transmission electron microscopy. The TEM images demonstrate that the majority of calcium carbonate nanoparticles have a significant propensity to aggregate due to their high surface energy, which results from their small particle size (Ghadami *et al.,* 2013).

According to TEM investigation, the synthesized CCNPs nanoparticles at various temperature had an average particle size of 44 ± 10 nm, 29± 4 nm and 105± 65 nm, which were consistent with the average crystal sizes estimated from the XRD data (Hari Bala *et al.,*2005). The synthesized CCNPs also showed that, at the same concentration, particle size varied with different temperatures. In comparison to the other two samples, the average particle size at 50°C was determined to be the lowest, supporting the findings of the XRD study.

In the results of the TEM study, the synthesized CCNPs nanoparticles at various temperatures exhibited a rod-like structure and were properly crystallized.

Chapter 6: Conclusion

In conclusion, $CaCO_3$ nanoparticles could have implicit places in unborn therapeutic operations due to bio-accessibility, bio-availability and it's economically affordable. Their role in bone scaffolding, tissue engineering, gene and medicine delivery is important and could replace numerous old ways and treatment styles in conditions similar as cancer microbial infections. The use of calcium carbonate nanoparticles in poultry feed can ameliorate the digestibility and immersion of nutrients, leading to bettered growth and productivity in poultry. As a feed supplement the use of calcium carbonate nanoparticles also offers environmental benefits, because it can reduce the quantum of waste generated by the poultry industry. At low concentrations the nanoparticles can be incorporated into feed formulations, which can drop the quantum of redundant nutrients excreted by poultry into the environment. Overall, the synthesis and characterization of calcium carbonate nanoparticles offer a promising result to ameliorate the effectiveness and sustainability of the poultry and dairy industry. To optimize the synthesis process and estimate the long- term effects of calcium carbonate nanoparticles more exploration is demanded on animal health and performance.

Chapter 7: Recommendations and Future Perspectives

The aim of synthesizing and characterizing calcium carbonate nanoparticles for use in the dairy and poultry industry as a feed additive for improving the overall health and productivity of these animals. Calcium carbonate is a very essential nutrient which is important for bone formation, eggshell formation and milk production. The surface area of the calcium carbonate can be increased by using nanoparticles, which enhances its absorption and bioavailability.

a. The effect of the synthesized nanoparticles on the growth performance, bone strength, eggshell quality and milk production of dairy and poultry animals can be investigated.

b. The safety and toxicity of the synthesized nanoparticles by conducting toxicity tests on animals can be assessed and the nanoparticles accumulation in organs is also can be analyzed.

c. To achieve the maximum benefit without adverse effects the dosage of the synthesized nanoparticles may be optimized.

Drug may be used with porous calcium carbonate and porous calcium carbonate will work as feed and as drug loader simultaneously.

References

Akter, M., Ullah, A. K. M. A., Rahaman, S., Rahman, M. and Sikder, T. (2019). Stability Enhancement of Silver Nanoparticles Through Surface Encapsulation via a Facile Green Synthesis Approach and Toxicity Reduction. Journal of Inorganic and Organometallic Polymers and Materials, 0123456789.

Amerah, A. M., Ravindran, V. and Lentle, R. G. (2017). Influence of particle size and coating of calcium carbonate on the apparent digestibility of calcium in broiler chickens. Poultry science, 96(3), 657-665.

Al-Mufarrej, S. I., Al-Abdullatif, A. A., Al-Sheikhly, F. A. and Al-Fataftah, A. R. (2019). The impact of nano-calcium carbonate supplementation on the immune response of broiler chickens. International Journal of Poultry Science, 18(5), 217-222.

Anandalaksmi, K., Venugobal, J. and Ramasamy, V. (2015). Characterization of Silver nanoparticles by green synthesis method using *Pedalium murex* leaf extract and their antibacterial activity. Appl Nanosci, DOI 10.1007/s 13204-015-0449-z.

Ali Said, F., Bousserrhineb, N., Alphonse, V., Michely, L. and Belbekhouche, S. (2020). Antibiotic loading and development of antibacterial capsules by using porous $CaCO_3$ microparticles as starting material. International Journal of Pharmaceutics 579 (2020) 119175.

Atta, A. M., Al-Lohedan, H. A., Ezzat, A. O. and Al-Hussain, S. A. (2016). Characterization of superhydrophobic epoxy coatings embedded bymodified calcium carbonate nanoparticles. Progress in Organic Coatings 101 (2016) 577–586.

Aydın,C., Yakuphanoglu, F. and Aydın, H. (2018). Al-doped ZnO as a multifunctional nanomaterial: Structural, morphological, optical and low-temperature gas sensing properties. *Journal of Alloys and Compounds*, *773*, 802–811.

Bashir, S., Khan, S., Zaneb, H. and Lee, H. J. (2018). Effects of nano-calcium carbonate on eggshell quality, mineral deposition, and bone metabolism in laying hens. Journal of Applied Poultry Research, 27(2), 257-266.

Bar, Harekrishna., Bhui, D.K., Sahoo, G.P. and Misra, A. (2009). Green synthesis of silver nanoparticles using latex of *Jatropa curcas*. Colloids and Surfaces A: Physicochem.Eng.Aspects 339,(134-139).

Biradar, S., Ravichandran, P., Gopikrishnan, R., Goornavar, V., Hall, C. J., Ramesh, V., Baluchamy, S., Jeffers, R. B. and Ramesh, G. T. (2011). Calcium Carbonate Nanoparticles: Synthesis, Characterization and Biocompatibility. J. Nanosci. Nanotechnol. Vol. 11, No. 8.

Chekli, L., Bayatsarmadi, B., Sekine, R., Sarkar, B., Shen, A. M., Scheckel, K. G., Skinner, W., Naidu, R., Shon, H. K., Lombi, E. and Donner, E. (2016). Analytical characterisation of nanoscale zero-valent iron: A methodological review. *Analytica Chimica Acta*, *903*, 13–35.

Diningsih, C. and Rohmawati, L. (2022). "Synthesis of Calcium Carbonate (CaCO3) from Eggshell by Calcination Method", Indonesian Physical Review, vol. 5, no. 2, p 208-215.

Dehghani, F., Kalantarias, A., Saboori, R., Sabbaghi, S. and Peyvandi, K.(2019). Performance of carbonate calcium nanoparticles as filtration loss control agent of water-based drilling fluid. SN Applied Sciences 1:1466.

Gupta,U., Vivek, K., Kumar, V. and Khajuria, Y. (2015). Experimental and theoretical spectroscopic studies of calcium carbonate (CaCO3). Materials Focus, Vol. 4, pp. 164–169.

Ghadami,J,G., Taleb,A., Idrees. and Mohammad. (2013). Characterization of $CaCO_3$ nanoparticles synthesized by reverse microemulsion technique in different concentrations of surfactants. Iran. J. Chem. Chem. Eng. Vol. 32, No.3.

Gabbasov, R., Polikarpov, M., Cherepanov, V., Chuev, M., Mischenko, I., Lomov, A., Wang, A. and Panchenko, V. (2015). Mössbauer, magnetization and X-ray diffraction characterization methods for iron oxide nanoparticles. *Journal of Magnetism and Magnetic Materials*, *380*, 111–116.

Hassanpour, H., Toghyani, M. and Shabani, A. (2016). Effect of dietary nano-calcium carbonate on performance, egg quality, tibia characteristics and blood parameters of laying hens. Journal of animal physiology and animal nutrition, 100(2), 297-304.

Hariharan, M., Varghese, N., Cherian, D. A. B., Sreeniasan,D. P.V., Paul,J. and Antony, A. (2014). Synthesis and Characterization of CaCO3 (Calcite) Nano Particles from Cockle Shells Using Chitosan as Precursor. International Journal of Scientific and Research Publications, Volume 4, ISSN 2250-315.

Hari-Bala, K., Ding, X., Guo,Y., Deng,Y., Wang,C., Li, M. and Wang, Z. (2015). Multigram scale synthesis and characterization of monodispersed cubic calcium carbonate nanoparticles. Materials Letters 60 (2006) 1515–1518.

Haefeli, C., Franklin, C. and Hardy, K. (1984). Plasmid-determined silver resistance in Pseudomonas stutzeri isolated from a silver mine. J Bacteriol 158:389–392.

Joy Prabu, H. and Johnson, I. (2015). Plant-Mediated Biosynthesis and Characterization of Silver Nanoparticles by Leaf Extracts of Tragia involucrata, Cymbopogon citronella, Solanum verbascifolium and Tylophora ovate. Karbala International Journal of Modern Science, 1, 237-246.

Kolahalam, L. A., Kasi Viswanath, I. V., Diwakar, B. S., Govindh, B., Reddy, V. and Murthy, Y. L. N. (2019). Review on nanomaterials: Synthesis and applications. *Materials Today: Proceedings*, *18*, 2182–2190.

Kandiah, M. and Chandrasekaran, K. N. (2021). Green Synthesis of Silver Nanoparticles Using Catharanthus roseus Flower Extracts and the Determination of Their Antioxidant, Antimicrobial, and Photocatalytic Activity. Journal of Nanotechnology, 2021.

Kazemi,M., Akbari, A.,Sabouri, Z. and Zarrinafar, H. (2021). Green synthesis of colloidal selenium nanoparticles in starch solutions and investigation of their photocatalytic, antimicrobial and cytotoxicity effects. Bioprocess and Biosystems Engineering.

Kabir, M. F., Ullah, A. K. M. A., Ferdousy, J. and Rahman, M. M. (2020). Anticancer efficacy of biogenic silver nanoparticles in vitro. *SN Applied Sciences*, *2*(6).

Kadota, K., Ibe, T., Sugawara, Y., Takano, H., Yusof, Y. A., Uchiyama, H., Tozuka, Y. and Yamanaka, S. (2020). Water-assisted synthesis of mesoporous calcium carbonate with a controlled specific surface area and its potential to ferulic acid release. RSC Adv., 2020, 10, 28019.

Lee, J. Y., Kim, Y. Y. and Kim, I. H. (2018). Effects of nano-calcium carbonate on animal performance, eggshell quality, and eggshell ultrastructure of laying hens. Journal of Animal Science and Biotechnology, 9(1), 13.

Lee, S. K. and McLaurin, E. J. (2018). Recent advances in colloidal indium phosphide quantum dot production. *Current Opinion in Green and Sustainable Chemistry*, *12*, 76–82.

Luo, X., Song, X., Cao, Y., Song, L. and Bu, X. (2020). Investigation of calcium carbonate synthesized by steamed ammonia liquid waste without use of additives. RSC Adv., 2020, 10, 7976.

Maleki,D. S., Barzegar,J. M., Zarrintan, M. H., Adibkia, K. and Lotfipour, F. (2015). Calcium carbonate nanoparticles as cancer drug delivery system. Expert Opin. Drug Deliv. 12, 1649-1660.

Majdoub, A., Gohar, Y. M. and Obeidat, B. S. (2016). The impact of high levels of nano-calcium carbonate on broiler performance and intestinal morphology. Poultry Science, 95(11), 2564-2571.

Majdoub, A., Mani, V., Kellingray, L., Symonds, M. E. and Lucas, A. (2017). Effects of dietary supplementation of nano-calcium carbonate or nano-calcium citrate on blood metabolites, egg quality, and immune response of laying hens. Journal of Dairy Science, 100(8), 6475-6483.

Mahdavi, A. H., Rahmani, H. R., Khajali, F. and Qujeq, D. (2019). Effect of nano-calcium carbonate on egg production, egg quality traits, and some blood biochemical parameters in laying hens. Journal of Dairy Science, 105(9), 7415-658.

Mandal, D., Bolander, M.E., Mukhopadhyay, D., Sarkar, G. and Mukherjee, P. (2006). The use of microorganisms for the formation of metal nanoparticles and their application. Appl Microbiol Biotechnol.Jan;69(5):485-92.

Mittal, A.K., Chisti, Y. and Banerjee, U.C. (2013). Synthesis of metallic nanoparticles using plant extracts. Biotechnol Adv.Mar-Apr;31(2):346-56.

Mensah, K., Abdelmageed, A. M. and Shokry, H. (2022). Effect of eggshell/N, N-dimethylformamide (DMF) mixing ratios on the sonochemical production of $CaCO_3$ nanoparticles. Mensah et al. Journal of Engineering and Applied Science 69:16.

Nagarajan, R. (2008). Nanoparticles: Building blocks for nanotechnology. ACS Symposium Series, 996, 2–14.

Nakkala, J. R., Mata, R. and Sadras, S. R. (2016). The antioxidant and catalytic activities of green synthesized gold nanoparticles from Piper longum fruit extract. Process Safety and Environmental Protection, 100, 288–294.

Nasseh, M. (2021). Improved Reverse Micelle method for the green synthesis of pH sensitive solid CaCO3 micro/nano scale particles. Department of Physics, Energy Studies and Nanotechnology, Murdoch University, Perth, Western Australia.

Preetha, D., Arun, R., Kumari, P. and Aarti, C. (2013). Synthesis and characterization of silver nanoparticles using cannonball leaves and their cytotoxic activity against Mcf-7 cell line. Journal of Nanotechnology, 2013, 1–5.

Pal, G., Alemany, L. B., Ci, L. and Ajayan, P. M. (2019). New insights into the structure and reduction of graphite oxide. *Nature Chemistry*, *1*(5), 403–408.

Park, W. M. and Champion, J. A. (2016). Colloidal assembly of hierarchically structured porous super particles from flower-shaped protein-inorganic hybrid nanoparticles. ACS Nano, 10, 8271-8280.

Prasad, P.N. (2012). Introduction to Nanomedicine and Nanobioengineering. Wiley Interscience: Hoboken, NJ.

Preetha, D., Arun, R., Kumari, P. and Aarti, C. (2013). Synthesis and characterization of silver nanoparticles using cannonball leaves and their cytotoxic activity against Mcf-7 cell line. *Journal of Nanotechnology*, *2013*, 1–5.

Rabiatul,B.,Mydin,S.M.N.,Izzah,N.Z.,Nurul,N.I.,Shaida,N.,Ghazali,N.S.,Moshawih,S .and Siddiquee, S. (2018). Potential of Calcium Carbonate Nanoparticles for Therapeutic Applications Malaysian Journal of Medicine and Health Sciences (eISSN 2636-9346). Mal J Med Health Sci 14(SUPP1): 201-206.

Rajabi, H. R., Karimi, F., Kazemdehdashti, H. and Kavoshi, L. (2018). Fast sonochemically-assisted synthesis of pure and doped zinc sulfide quantum dots and their applicability in organic dye removal from aqueous media. *Journal of Photochemistry and Photobiology B: Biology*, *181*(2017), 98–105.

Rafique, M., Sadaf, I., Rafique, M.S. and Tahir, M.B. (2017). A review on green synthesis of silver nanoparticles and their applications. Artif Cells Nanomed Biotechnol. Nov;45(7):1272-1291.

Rai, M., Yadav, A. and Gade, A. (2008). Silver nanoparticles as a new generation of antimicrobials. Biotechnol Adv. Jan-Feb;27(1):76-83.

Riehemann, K., Schneider,S.W., Luger, T.A., Godin, B., Ferrari, M. and Fuchs, H. (2009). Nanomedicine-Challenge and Perspectives. Angew, Chem., Int. Ed; 48 (5): 872−897.

Sharma, V. K., Yngard, R. A. and Lin, Y. (2009). Silver nanoparticles: Green synthesis and their antimicrobial activities. *Advances in Colloid and Interface Science*, *145*(1–2), 83–96.

Shivaraj, Y., Siddegowda, K. S. and Mallappa, M. (2017). Calcium Carbonate Nanoparticles Enhanced Electrochemical Sensing of DNA. Arch. Appl. Sci. Res., 9 (1):44-5.

Singh, P., Kim, Y. J., Zhang, D. and Yang, D.C. (2016). Biological Synthesis of Nanoparticles from Plants and Microorganisms. Trends Biotechnol. Jul;34(7):588-599.

Sathishkumar, M., Sneha, K., Won, S. W., Kim, S. and Yun, Y. S. (2009). *Cinnamon zeylanicum* bark extract and powder mediated green synthesis of nano-crystalline silver particles and its bactericidal activity. Colloids and Surfaces B: Biointerfaces 73 (2009) 332-338.

Shafaghat. (2015). Synthesis and Characterization of Silver Nanoparticles by Phytosynthesis Method and their Biological Activity Synthesis and Characterization of Silver Nanoparticles by Phytosynthesis Method. *Synthesis and Reactivity in Inorganic, Metal-Organic and Nano-Metal Chemistry*, *45(3)* (November 2014), 381–387.

Uddin, A. K. M. R., Bakar, A., Farjana, S., Atique, R. A. K. M. and Khan, R. (2020). Cocos nucifera Leaf Extract Mediated Green Synthesis of Silver Nanoparticles for Enhanced Antibacterial Activity. *Journal of Inorganic and Organometallic Polymers and Materials 4*(11), 12054–12060.

Wang, J., Kong, Y., Liu, F., Shou, D., Tao, Y. and Qin, Y. (2018). Construction of P^H -responsive drug delivery platform with calcium carbonate microspheres induced by chitosan gels. Ceramics international.

Xuan, Y., Zhang, X., Sun, L., Wei, Y. and Wei, X. (2019). Cellular Toxicity and Immunological Effects of Carbon-based Nanomaterials. *Particle and Fibre Toxicology*, *16*(1).

Xiang, Y., Han, J., Zhang, G., Zhan, F., Cai, D. and Wu, Z. (2018). Efficient synthesis of starch regulated porous calcium carbonate microspheres as a carrier for slow-release herbicide. ACS sustainable chem. Eng.

Xue, Z., Hu, B., Dai, S. and Du, Z. (2015). Transformation of amorphous calcium carbonate to rod-like single crystal calcite via "copying" collagen template. Materials Science and Engineering C55 (2015) 506–511.

Yue, L. Y., Zhang, Z. C. and Chen, X. (2006). Absorption and fluorescence spectra of gallium phosphide (GaP) nanoparticles. *Transactions of Nonferrous Metals Society of China (English Edition)*, *16*(4), 863–867.

Appendices

Appendix A: S-0.25(20)-Evaluation report

General information

Name	Value	Name	Value
Analysis date	2023-07-16 10:42:07	Measurement star	2023-05-02 12:49:41
Analyst	Administrator	Operator	Administrator
Sample name		Comment	
Measured data n	E:\Data from XRD\SERVICE DATA\2	Memo	

Measurement Conditions

Name	Value	Name	Value
X-Ray generator	40 kV, 40 mA	Scan mode	1D(scan)
Incident primary	Standard	Scan speed/Durati...	5.00 °/min
Goniometer	Standard Goniometer	Step width	0.02 °
Attachment	Standard	Scan axis	θ/2θ
Filter	Kβ filter 1D for Cu	Scan range	5 ~ 80 °
Selection slit	PB	Incident slit box	1.000mm
Diffracted beam...	None	Length-limiting slit	10 mm
Detector	D/teX Ultra 250 (H)	Receiving slit box...	Open
Optics attribute	PB	Receiving slit box...	Open

Measured profile view

Peak

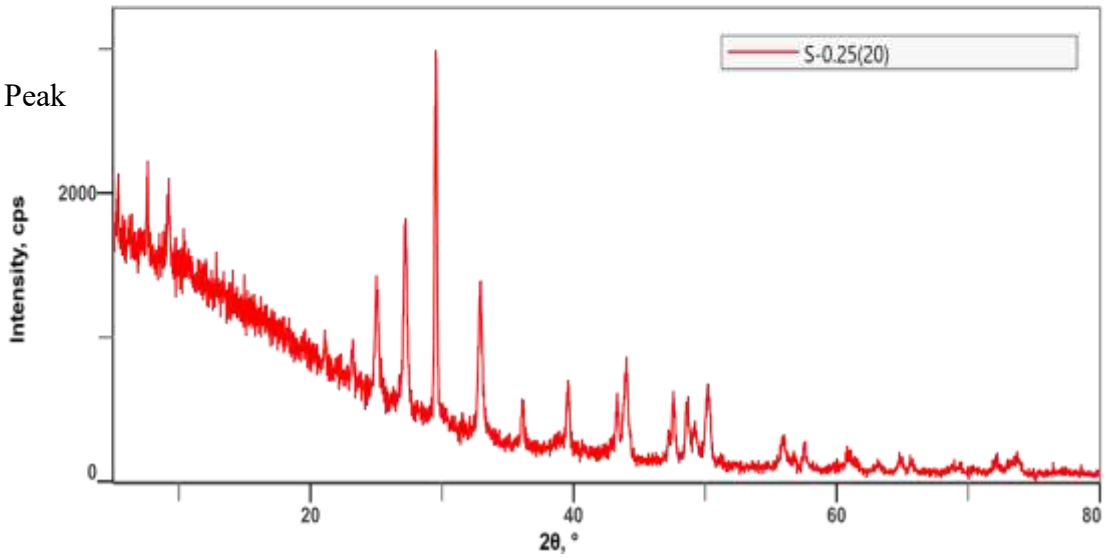

Profiling conditions

Peak Profile View

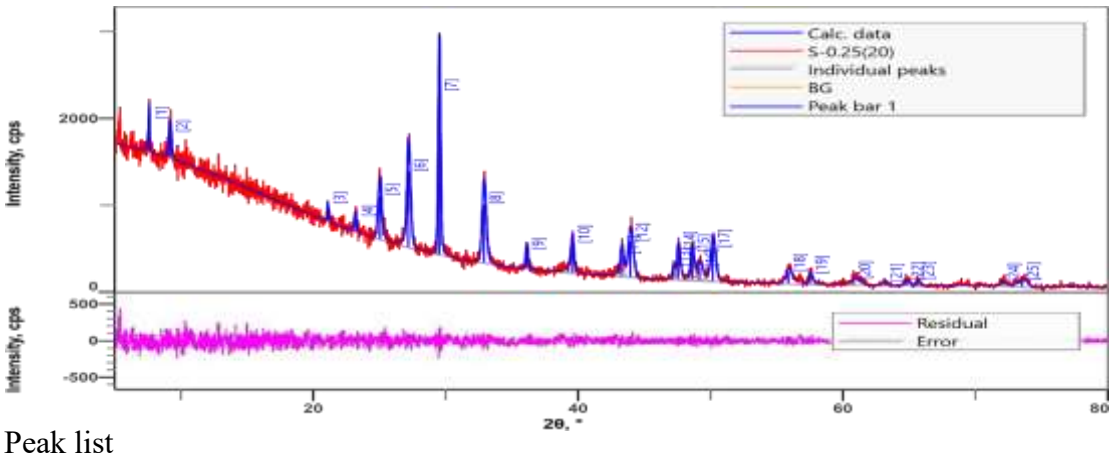

Peak list

No.	2θ, °	d, Å	Height, cps	FWHM, °	Int. I., cps°	Int. W., °	Asymmetry
1	7.624(6)	11.586(9)	375(16)	0.11(2)	58(8)	0.15(3)	3(7)
2	9.20(3)	9.60(3)	297(14)	0.23(3)	79(11)	0.27(5)	1.3(8)
3	21.08(2)	4.212(4)	195(12)	0.08(4)	27(5)	0.14(3)	1.0(12)
4	23.21(2)	3.829(4)	169(11)	0.18(3)	36(6)	0.21(5)	3(2)
5	25.02(2)	3.556(3)	503(28)	0.300(19)	183(10)	0.36(4)	1.4(4)
6	27.155(12)	3.2812(14)	873(43)	0.295(10)	326(8)	0.37(3)	0.78(14)
7	29.491(8)	3.0264(8)	1881(74)	0.179(6)	411(8)	0.218(13)	1.2(2)
8	32.866(16)	2.7229(13)	674(40)	0.336(13)	271(9)	0.40(4)	1.02(19)
9	36.07(4)	2.488(2)	214(18)	0.19(2)	43(5)	0.20(4)	1.0(7)
10	39.551(17)	2.2767(10)	342(26)	0.22(4)	125(6)	0.37(5)	2.8(16)
11	43.236(14)	2.0908(6)	255(24)	0.21(3)	72(6)	0.28(5)	0.9(2)
12	43.91(2)	2.0604(10)	412(30)	0.41(3)	222(8)	0.54(6)	0.9(2)
13	47.155(13)	1.9258(5)	155(17)	0.13(3)	29(5)	0.19(6)	0.8(3)
14	47.505(17)	1.9124(6)	349(29)	0.21(2)	105(7)	0.30(4)	0.8(3)
15	48.558(14)	1.8734(5)	317(27)	0.24(2)	102(6)	0.32(5)	0.9(2)
16	49.13(3)	1.8530(10)	158(17)	0.43(5)	93(6)	0.59(10)	0.9(2)
17	50.12(2)	1.8185(7)	386(33)	0.37(2)	192(6)	0.50(6)	0.9(2)
18	55.815(15)	1.6458(4)	136(15)	0.52(5)	119(5)	0.88(14)	0.6(3)
19	57.46(4)	1.6025(10)	115(12)	0.24(6)	36(4)	0.31(7)	1.0(9)
20	60.76(3)	1.5231(8)	64(9)	0.77(9)	67(6)	1.1(2)	0.5(3)
21	63.13(3)	1.4715(6)	40(7)	0.30(8)	15(3)	0.38(15)	4(7)
22	64.73(6)	1.4390(12)	59(9)	0.33(7)	24(3)	0.41(10)	1.2(9)
23	65.53(3)	1.4233(5)	66(10)	0.15(3)	12.3(17)	0.19(6)	1.2(9)
24	71.99(11)	1.3107(17)	49(8)	0.32(10)	17(4)	0.35(14)	1.2(16)

Name	Value	Name	Value	Name	Value
Peak search	Second derivative.m	σ cut	3.00		
Profile fitting	Run completed	Peak shape	Split pseudo-Voigt	Fitting condition	Auto(Refine background)

No.	2θ, °	Decay(ηL/mL)	Decay(ηH/mH)	Size, Å	Phase Name	Chemical Formula
1	7.624(6)	0.6(5)	1.1(5)	769(157)	Unknown: 0 0 0	
2	9.20(3)	0.0(7)	0.4(7)	355(43)	Unknown: 0 0 0	
3	21.08(2)	0.6(13)	1.5(8)	1070(492)	Unknown: 0 0 0	
4	23.21(2)	0.0(6)	0.8(10)	458(82)	Calcium Carbonate: 0 1 2	Ca (C O3)
5	25.02(2)	0.0(3)	0.8(3)	283(18)	Unknown: 0 0 0	
6	27.155(12)	0.73(15)	0.27(12)	289(10)	Unknown: 0 0 0	
7	29.491(8)	0.26(9)	0.56(12)	480(15)	Calcium Carbonate: 1 0 4	Ca (C O3)
8	32.866(16)	0.26(16)	0.42(16)	257(10)	Unknown: 0 0 0	
9	36.07(4)	0.0(6)	0.0(6)	466(62)	Calcium Carbonate: 1 1 0	Ca (C O3)
10	39.551(17)	1.1(3)	1.4(4)	410(69)	Calcium Carbonate: 1 1 3	Ca (C O3)
11	43.236(14)	1.1(2)	0.01(15)	421(67)	Calcium Carbonate: 2 0 2	Ca (C O3)
12	43.91(2)	1.1(2)	0.01(15)	221(14)	Unknown: 0 0 0	
13	47.155(13)	0.9(3)	0.7(2)	685(174)	Calcium Carbonate: 0 2 4	Ca (C O3)
14	47.505(17)	0.9(3)	0.7(2)	427(48)	Calcium Carbonate: 0 1 8	Ca (C O3)
15	48.558(14)	0.75(17)	0.58(15)	385(35)	Calcium Carbonate: 1 1 6	Ca (C O3)
16	49.13(3)	0.75(17)	0.58(15)	211(22)	Unknown: 0 0 0	
17	50.12(2)	0.75(17)	0.58(15)	249(13)	Unknown: 0 0 0	
18	55.815(15)	1.04(19)	1.2(3)	180(17)	Unknown: 0 0 0	
19	57.46(4)	0.0(7)	1.0(7)	397(102)	Calcium Carbonate: 1 2 2	Ca (C O3)
20	60.76(3)	1.4(2)	0.0(4)	125(15)	Calcium Carbonate: 2 1 4	Ca (C O3)
21	63.13(3)	0.0(10)	1.5(6)	330(93)	Calcium Carbonate: 1 2 5	Ca (C O3)
22	64.73(6)	0.0(6)	0.8(7)	296(62)	Calcium Carbonate: 3 0 0	Ca (C O3)
23	65.53(3)	0.0(6)	0.8(7)	646(135)	Calcium Carbonate: 0 0 12	Ca (C O3)
24	71.99(11)	0.0(11)	0.3(13)	322(103)	Unknown: 0 0 0	

No.	2θ, °	Card No	Norm. I.	Profile Type	Distributi...	Degree of Orientation
1	7.624(6)		14.11	Split pseudo-Voigt	-	-
2	9.20(3)		19.31	Split pseudo-Voigt	-	-
3	21.08(2)		6.47	Split pseudo-Voigt	-	-
4	23.21(2)	01-080-9776	8.77	Split pseudo-Voigt	-	-
5	25.02(2)		44.66	Split pseudo-Voigt	-	-
6	27.155(12)		79.35	Split pseudo-Voigt	-	-
7	29.491(8)	01-080-9776	100.00	Split pseudo-Voigt	-	-
8	32.866(16)		65.97	Split pseudo-Voigt	-	-
9	36.07(4)	01-080-9776	10.38	Split pseudo-Voigt	-	-
10	39.551(17)	01-080-9776	30.49	Split pseudo-Voigt	-	-
11	43.236(14)	01-080-9776	17.50	Split pseudo-Voigt	-	-
12	43.91(2)		54.04	Split pseudo-Voigt	-	-
13	47.155(13)	01-080-9776	7.05	Split pseudo-Voigt	-	-
14	47.505(17)	01-080-9776	25.52	Split pseudo-Voigt	-	-
15	48.558(14)	01-080-9776	24.72	Split pseudo-Voigt	-	-
16	49.13(3)		22.57	Split pseudo-Voigt	-	-
17	50.12(2)		46.86	Split pseudo-Voigt	-	-
18	55.815(15)		29.01	Split pseudo-Voigt	-	-
19	57.46(4)	01-080-9776	8.73	Split pseudo-Voigt	-	-
20	60.76(3)	01-080-9776	16.33	Split pseudo-Voigt	-	-
21	63.13(3)	01-080-9776	3.69	Split pseudo-Voigt	-	-
22	64.73(6)	01-080-9776	5.87	Split pseudo-Voigt	-	-
23	65.53(3)	01-080-9776	3.00	Split pseudo-Voigt	-	-
24	71.99(11)		4.22	Split pseudo-Voigt	-	-

No.	2θ, °	Ring Factor	β Cluster
1	7.624(6)	-	-
2	9.20(3)	-	-
3	21.08(2)	-	-
4	23.21(2)	-	-
5	25.02(2)	-	-
6	27.155(12)	-	-
7	29.491(8)	-	-
8	32.866(16)	-	-
9	36.07(4)	-	-
10	39.551(17)	-	-
11	43.236(14)	-	-
12	43.91(2)	-	-
13	47.155(13)	-	-
14	47.505(17)	-	-
15	48.558(14)	-	-
16	49.13(3)	-	-
17	50.12(2)	-	-
18	55.815(15)	-	-
19	57.46(4)	-	-
20	60.76(3)	-	-
21	63.13(3)	-	-
22	64.73(6)	-	-
23	65.53(3)	-	-
24	71.99(11)	-	-

Qualitative analysis results

Phase name	Formula	Figure of merit	Phase reg. detail	Space Group	DB Card Number
Calcium Carbonate	Ca (C O3)	1.024	S/M(PDF-2 Releas...	167 : R-3c:H	01-080-9776

Phase Data View

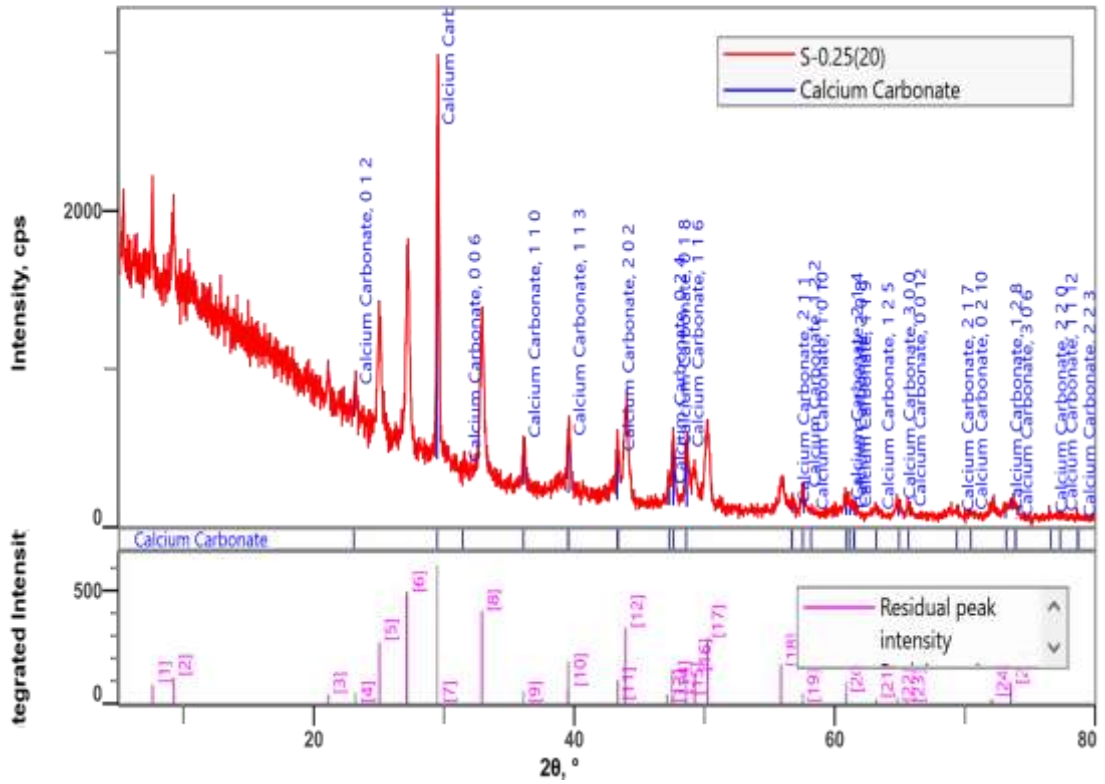

Lattice parameters

Phase name	a, Å	b, Å	c, Å	α, °	β, °	γ, °
Calcium Carbc	4.97738	4.97738	17.04989	90.000	90.000	120.000

d-I List

Calcium Carbonate

No.	2θ, °	d, Å	h k l	Norm. I.
1	23.10270	3.84675	0 1 2	9.40
2	29.44644	3.03087	1 0 4	100.00
3	31.45636	2.84165	0 0 6	1.90
4	36.06045	2.48869	1 1 0	13.90
5	39.49718	2.27970	1 1 3	17.00
6	43.26435	2.08953	2 0 2	14.30
7	47.21790	1.92337	0 2 4	6.20
8	47.55625	1.91048	0 1 8	17.50
9	48.59065	1.87220	1 1 6	17.60
10	56.71235	1.62184	2 1 1	2.70
11	57.54780	1.60027	1 2 2	7.60
12	58.13605	1.58547	1 0 10	0.90
13	60.81649	1.52185	2 1 4	4.30
14	61.10130	1.51544	2 0 8	1.80
15	61.46265	1.50739	1 1 9	2.00
16	63.20062	1.47006	1 2 5	1.60
17	64.83737	1.43685	3 0 0	4.80
18	65.65994	1.42082	0 0 12	2.60
19	69.33563	1.35421	2 1 7	0.80
20	70.34837	1.33717	0 2 10	1.30
21	73.04270	1.29435	1 2 8	2.10
22	73.84559	1.28225	3 0 6	0.40
23	73.84559	1.28225	0 3 6	0.00
24	76.49174	1.24435	2 2 0	0.90
25	77.25879	1.23389	1 1 12	1.40
26	78.64748	1.21555	2 2 3	0.10

Appendix B: S-0.25(50)-Evaluation report

General information

Name	Value	Name	Value
Analysis date	2023-07-16 10:43:10	Measurement star	2023-05-02 13:08:19
Analyst	Administrator	Operator	Administrator
Sample name		Comment	
Measured data.n	E:\Data from XRD\SERVICE DATA\2	Memo	

Measurement Conditions

Name	Value	Name	Value
X-Ray generator	40 kV, 40 mA	Scan mode	1D(scan)
Incident primary	Standard	Scan speed/Durati...	5.00 °/min
Goniometer	Standard Goniometer	Step width	0.02 °
Attachment	Standard	Scan axis	θ/2θ
Filter	Kβ filter 1D for Cu	Scan range	5 – 80 °
Selection slit	PB	Incident slit box	1.000mm
Diffracted beam...	None	Length-limiting slit	10 mm
Detector	D/teX Ultra 250 (H)	Receiving slit box...	Open
Optics attribute	PB	Receiving slit box...	Open

Measured profile view

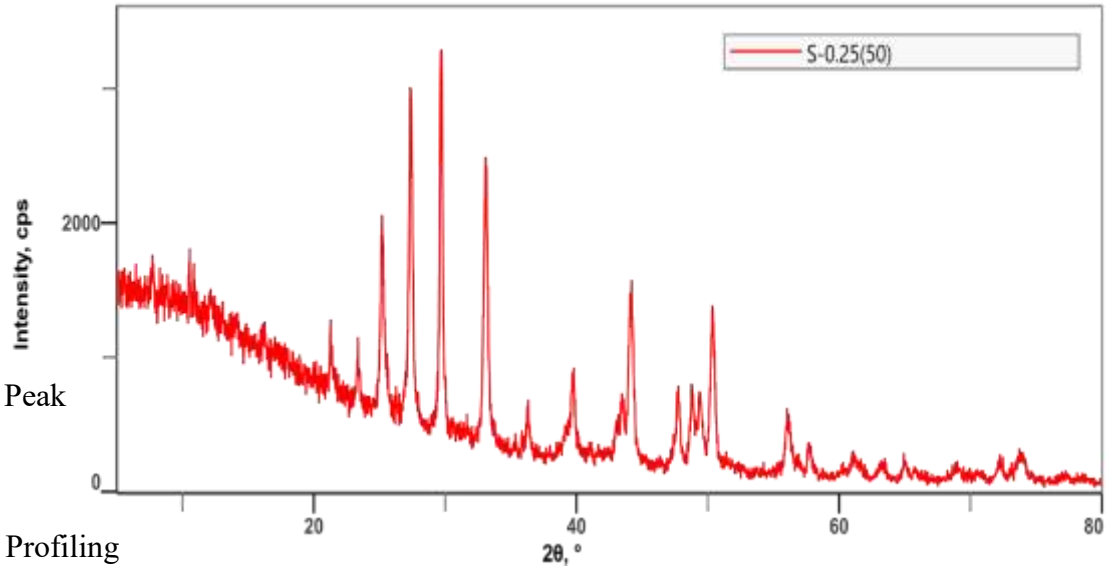

Peak Profiling conditions

Name	Value	Name	Value	Name	Value
Peak search	Second derivative.m	σ cut	3.00		
Profile fitting	Run completed	Peak shape	Split pseudo-Voigt	Fitting condition	Auto(Refine background)

Peak Profile View

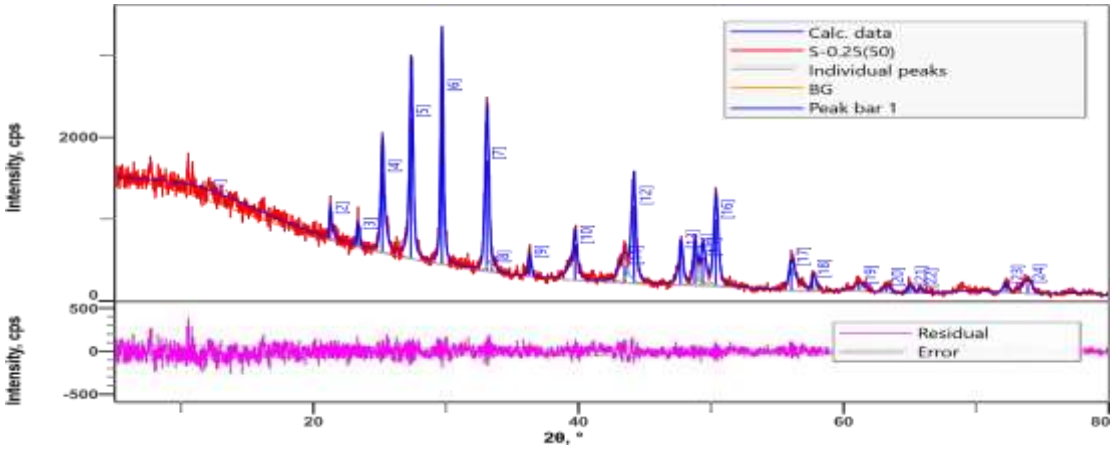

Peak list

No.	2θ, °	d, Å	Height, cps	FWHM, °	Int. I., cps°	Int. W., °	Asymmetry
1	11.99(18)	7.38(11)	90(5)	9.6(5)	964(45)	10.8(11)	0.59(13)
2	21.222(8)	4.1833(15)	310(19)	0.15(4)	85(7)	0.27(4)	0.6(5)
3	23.312(10)	3.8127(16)	203(13)	0.25(3)	54(7)	0.27(5)	0.7(4)
4	25.179(12)	3.5340(17)	980(44)	0.271(16)	415(11)	0.42(3)	1.2(3)
5	27.327(11)	3.2610(13)	1719(63)	0.281(10)	680(11)	0.40(2)	0.90(16)
6	29.660(10)	3.0095(10)	2106(78)	0.213(9)	625(10)	0.297(16)	1.4(3)
7	33.037(9)	2.7092(7)	1359(56)	0.326(7)	517(12)	0.38(2)	1.12(12)
8	33.4(2)	2.680(19)	105(9)	0.63(8)	77(10)	0.73(16)	1.12(12)
9	36.241(11)	2.4767(7)	218(17)	0.22(3)	63(6)	0.29(5)	0.8(8)
10	39.689(8)	2.2691(5)	437(30)	0.35(2)	291(9)	0.67(7)	1.7(7)
11	43.44(3)	2.0816(13)	216(16)	0.71(7)	225(21)	1.04(18)	2.5(2)
12	44.146(9)	2.0498(4)	951(50)	0.318(16)	441(23)	0.46(5)	2.5(2)
13	47.640(15)	1.9073(5)	436(33)	0.25(3)	186(6)	0.43(5)	0.71(19)
14	48.725(13)	1.8673(5)	394(29)	0.29(2)	158(8)	0.40(5)	1.3(2)
15	49.331(19)	1.8458(7)	348(26)	0.41(3)	195(9)	0.56(7)	1.3(2)
16	50.296(16)	1.8126(5)	818(47)	0.354(15)	396(8)	0.48(4)	1.3(2)
17	56.003(11)	1.6407(3)	297(24)	0.46(5)	232(7)	0.78(9)	0.9(3)
18	57.591(13)	1.5992(3)	147(15)	0.33(4)	54(5)	0.36(7)	0.5(3)
19	61.10(8)	1.5155(17)	68(9)	0.91(7)	66(5)	1.0(2)	1.0(3)
20	63.14(5)	1.4713(11)	63(9)	0.56(6)	37(3)	0.60(14)	1.0(3)
21	64.89(5)	1.4358(10)	91(12)	0.31(7)	36(4)	0.40(9)	1.1(8)
22	65.65(3)	1.4209(6)	64(10)	0.18(5)	14(2)	0.22(7)	1.1(8)
23	72.16(3)	1.3079(5)	96(17)	0.37(6)	38(3)	0.40(10)	1.9(6)
24	73.82(6)	1.2827(9)	118(14)	0.88(5)	111(7)	0.94(18)	1.9(6)

No.	2θ, °	Decay(ηL/mL)	Decay(ηH/mH)	Size, Å	Phase Name	Chemical Formula
1	11.99(18)	0.0(13)	0.24(17)	8.7(4)	Unknown: 0 0 0	
2	21.222(8)	0.6(5)	1.5(2)	547(132)	Unknown: 0 0 0	
3	23.312(10)	0.1(7)	0.0(6)	342(38)	Calcium Carbonate: 0 1 2	Ca (C O3)
4	25.179(12)	0.54(13)	1.37(16)	314(19)	Unknown: 0 0 0	
5	27.327(11)	0.89(12)	0.62(10)	304(10)	Unknown: 0 0 0	
6	29.660(10)	0.52(9)	0.98(17)	403(17)	Calcium Carbonate: 1 0 4	Ca (C O3)
7	33.037(9)	0.40(8)	0.1(2)	265(6)	Unknown: 0 0 0	
8	33.4(2)	0.40(8)	0.1(2)	138(18)	Unknown: 0 0 0	
9	36.241(11)	1.0(3)	0.0(5)	390(61)	Calcium Carbonate: 1 1 0	Ca (C O3)
10	39.689(8)	1.45(12)	1.29(11)	256(16)	Calcium Carbonate: 1 1 3	Ca (C O3)
11	43.44(3)	0.59(15)	1.3(3)	125(13)	Calcium Carbonate: 2 0 2	Ca (C O3)
12	44.146(9)	0.59(15)	1.3(3)	282(15)	Unknown: 0 0 0	
13	47.640(15)	1.55(19)	0.8(2)	364(38)	Calcium Carbonate: 0 1 8	Ca (C O3)
14	48.725(13)	0.51(11)	0.88(14)	310(23)	Calcium Carbonate: 1 1 6	Ca (C O3)
15	49.331(19)	0.51(11)	0.88(14)	223(15)	Unknown: 0 0 0	
16	50.296(16)	0.51(11)	0.88(14)	259(11)	Unknown: 0 0 0	
17	56.003(11)	0.83(15)	1.41(11)	206(21)	Unknown: 0 0 0	
18	57.591(13)	0.4(5)	0.0(4)	289(33)	Calcium Carbonate: 1 2 2	Ca (C O3)
19	61.10(8)	0.0(4)	0.0(4)	106(8)	Calcium Carbonate: 2 1 4	Ca (C O3)
20	63.14(5)	0.0(4)	0.0(4)	174(20)	Calcium Carbonate: 1 2 5	Ca (C O3)
21	64.89(5)	0.0(6)	0.9(6)	313(67)	Calcium Carbonate: 3 0 0	Ca (C O3)
22	65.65(3)	0.0(6)	0.9(6)	561(159)	Unknown: 0 0 0	
23	72.16(3)	0.0(3)	0.0(4)	274(41)	Unknown: 0 0 0	
24	73.82(6)	0.0(3)	0.0(4)	118(7)	Calcium Carbonate: 1 2 8	Ca (C O3)

No.	2θ, °	Card No	Norm. I.	Profile Type	Distributi...	Degree of Orientation
1	11.99(18)		100.00	Split pseudo-Voigt	-	-
2	21.222(8)		8.79	Split pseudo-Voigt	-	-
3	23.312(10)	01-080-9776	5.60	Split pseudo-Voigt	-	-
4	25.179(12)		43.03	Split pseudo-Voigt	-	-
5	27.327(11)		70.52	Split pseudo-Voigt	-	-
6	29.660(10)	01-080-9776	64.85	Split pseudo-Voigt	-	-
7	33.037(9)		53.60	Split pseudo-Voigt	-	-
8	33.4(2)		7.99	Split pseudo-Voigt	-	-
9	36.241(11)	01-080-9776	6.52	Split pseudo-Voigt	-	-
10	39.689(8)	01-080-9776	30.20	Split pseudo-Voigt	-	-
11	43.44(3)	01-080-9776	23.30	Split pseudo-Voigt	-	-
12	44.146(9)		45.75	Split pseudo-Voigt	-	-
13	47.640(15)	01-080-9776	19.26	Split pseudo-Voigt	-	-
14	48.725(13)	01-080-9776	16.43	Split pseudo-Voigt	-	-
15	49.331(19)		20.24	Split pseudo-Voigt	-	-
16	50.296(16)		41.04	Split pseudo-Voigt	-	-
17	56.003(11)		24.07	Split pseudo-Voigt	-	-
18	57.591(13)	01-080-9776	5.57	Split pseudo-Voigt	-	-
19	61.10(8)	01-080-9776	6.82	Split pseudo-Voigt	-	-
20	63.14(5)	01-080-9776	3.88	Split pseudo-Voigt	-	-
21	64.89(5)	01-080-9776	3.77	Split pseudo-Voigt	-	-
22	65.65(3)		1.48	Split pseudo-Voigt	-	-
23	72.16(3)		3.99	Split pseudo-Voigt	-	-
24	73.82(6)	01-080-9776	11.55	Split pseudo-Voigt	-	-

No.	2θ, °	Ring Factor	β Cluster
1	11.99(18)	-	-
2	21.222(8)	-	-
3	23.312(10)	-	-
4	25.179(12)	-	-
5	27.327(11)	-	-
6	29.660(10)	-	-
7	33.037(9)	-	-
8	33.4(2)	-	-
9	36.241(11)	-	-
10	39.689(8)	-	-
11	43.44(3)	-	-
12	44.146(9)	-	-
13	47.640(15)	-	-
14	48.725(13)	-	-
15	49.331(19)	-	-
16	50.296(16)	-	-
17	56.003(11)	-	-
18	57.591(13)	-	-
19	61.10(8)	-	-
20	63.14(5)	-	-
21	64.89(5)	-	-
22	65.65(3)	-	-
23	72.16(3)	-	-
24	73.82(6)	-	-

Qualitative analysis results

Phase name	Formula	Figure of merit	Phase reg. detail	Space Group	DB Card Number
Calcium Carbonate	Ca (C O3)	1.097	S/M(PDF-2 Releas…	167 : R-3c:H	01-080-9776

Phase Data View

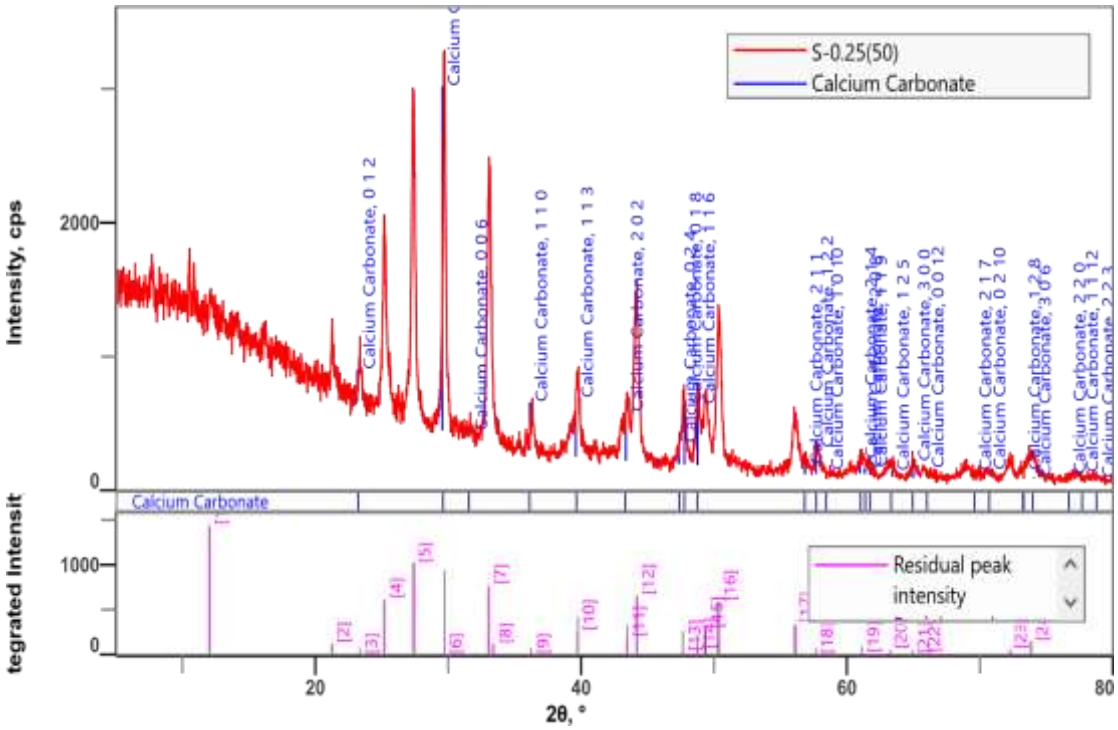

Lattice parameters

Phase name	a, Å	b, Å	c, Å	α, °	β, °	γ, °
Calcium Carbc	4.97169	4.97169	16.98146	90.000	90.000	120.000

d-I List
Calcium Carbonate

No.	2θ, °	d, Å	h k l	Norm. I.
1	23.14328	3.84010	0 1 2	9.40
2	29.52486	3.02300	1 0 4	100.00
3	31.58641	2.83024	0 0 6	1.90
4	36.10314	2.48585	1 1 0	13.90
5	39.56339	2.27604	1 1 3	17.00
6	43.32425	2.08678	2 0 2	14.30
7	47.30469	1.92005	0 2 4	6.20
8	47.73116	1.90388	0 1 8	17.50
9	48.71471	1.86772	1 1 6	17.60
10	56.78476	1.61995	2 1 1	2.70
11	57.62624	1.59828	1 2 2	7.60
12	58.36802	1.57972	1 0 10	0.90
13	60.91825	1.51955	2 1 4	4.30
14	61.27751	1.51150	2 0 8	1.80
15	61.66522	1.50292	1 1 9	2.00
16	63.31918	1.46759	1 2 5	1.60
17	64.92067	1.43520	3 0 0	4.80
18	65.95810	1.41512	0 0 12	2.60
19	69.49715	1.35145	2 1 7	0.80
20	70.58434	1.33328	0 2 10	1.30
21	73.23031	1.29150	1 2 8	2.10
22	73.99484	1.28003	3 0 6	0.40
23	73.99484	1.28003	0 3 6	0.00
24	76.59515	1.24292	2 2 0	0.90
25	77.56322	1.22981	1 1 12	1.40
26	78.76736	1.21400	2 2 3	0.10

Appendix C: S-0.25(80)-Evaluation report

General information

Name	Value	Name	Value
Analysis date	2023-07-16 10:40:24	Measurement star	2023-05-02 13:32:10
Analyst	Administrator	Operator	Administrator
Sample name		Comment	
Measured data n	E:\Data from XRD\SERVICE DATA\2	Memo	

Measurement Conditions

Name	Value	Name	Value
X-Ray generator	40 kV, 40 mA	Scan mode	1D(scan)
Incident primary	Standard	Scan speed/Durati...	5.00 °/min
Goniometer	Standard Goniometer	Step width	0.02 °
Attachment	Standard	Scan axis	θ/2θ
Filter	Kβ filter 1D for Cu	Scan range	5 – 80 °
Selection slit	PB	Incident slit box	1.000mm
Diffracted beam...	None	Length-limiting slit	10 mm
Detector	D/teX Ultra 250 (H)	Receiving slit box...	Open
Optics attribute	PB	Receiving slit box...	Open

Measured profile view

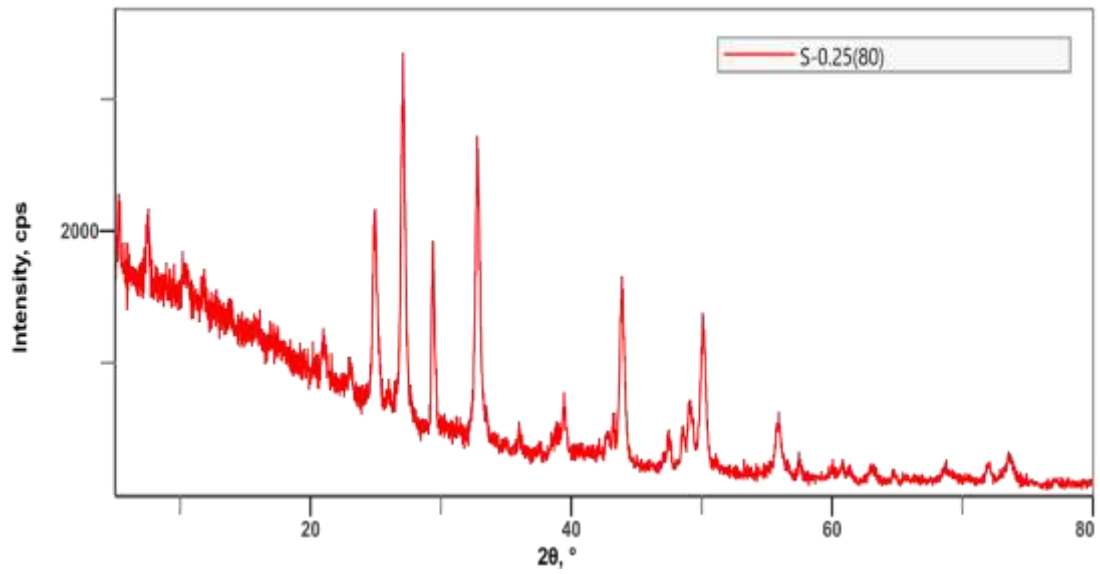

Peak profiling conditions

Name	Value	Name	Value	Name	Value
Peak search	Second derivative...m σ cut		3.00		
Profile fitting	Run completed	Peak shape	Split pseudo-Voigt	Fitting condition	Auto(Refine background)

Peak Profile View

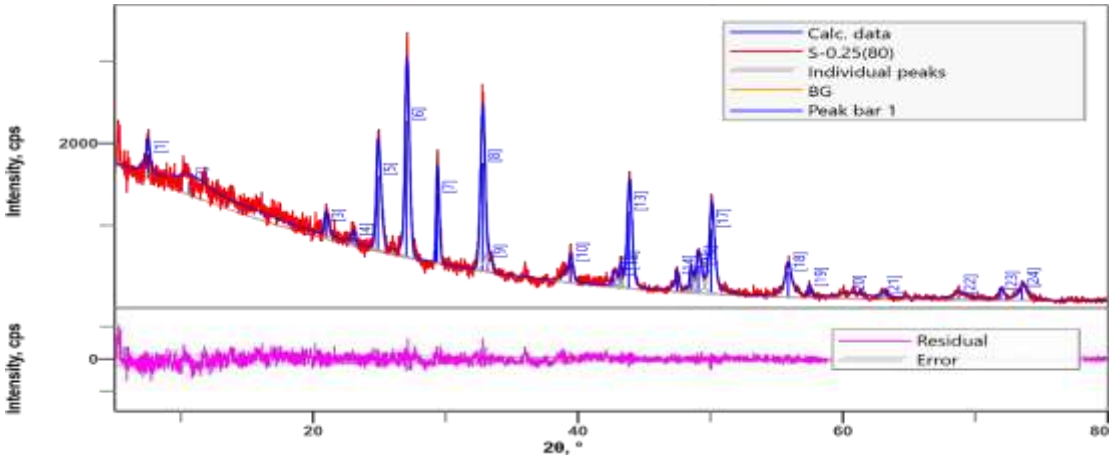

Peak list

No.	2θ, °	d, Å	Height, cps	FWHM, °	Int. I., cps°	Int. W., °	Asymmetry
1	7.531(18)	11.73(3)	299(14)	0.36(7)	181(20)	0.61(9)	1.1(15)
2	10.6(3)	8.3(2)	169(8)	4.4(4)	1473(61)	8.7(8)	0.50(18)
3	20.950(15)	4.237(3)	202(12)	0.37(5)	96(11)	0.48(8)	0.7(4)
4	23.01(2)	3.862(4)	112(7)	0.32(7)	44(9)	0.39(11)	1.2(12)
5	24.867(15)	3.578(2)	921(43)	0.407(13)	447(14)	0.49(4)	0.65(10)
6	27.011(11)	3.2984(14)	1660(62)	0.375(9)	728(16)	0.44(3)	0.60(8)
7	29.326(15)	3.0431(15)	848(42)	0.259(11)	234(11)	0.28(3)	0.61(14)
8	32.760(11)	2.7315(9)	1319(56)	0.389(9)	547(25)	0.41(4)	1.19(13)
9	33.15(19)	2.700(15)	171(12)	0.62(7)	113(18)	0.66(15)	1.19(13)
10	39.381(16)	2.2861(9)	250(21)	0.37(7)	171(11)	0.69(10)	1.4(9)
11	42.67(2)	2.1172(10)	126(12)	0.41(5)	67(6)	0.53(10)	0.69(11)
12	43.149(9)	2.0949(4)	210(19)	0.12(2)	34(4)	0.16(3)	0.69(11)
13	43.788(14)	2.0657(6)	940(49)	0.392(12)	478(8)	0.51(4)	0.69(11)
14	47.42(2)	1.9156(8)	207(19)	0.21(5)	85(5)	0.41(6)	1.8(10)
15	48.452(10)	1.8772(4)	231(22)	0.20(3)	64(6)	0.28(5)	0.96(16)
16	49.037(19)	1.8562(7)	338(26)	0.45(3)	212(9)	0.63(7)	0.96(16)
17	50.015(16)	1.8222(5)	798(44)	0.415(15)	467(10)	0.58(5)	0.96(16)
18	55.81(4)	1.6459(10)	307(27)	0.50(6)	274(8)	0.89(10)	1.3(5)
19	57.39(3)	1.6043(9)	128(15)	0.18(4)	30(4)	0.24(6)	1.2(11)
20	60.27(9)	1.534(2)	44(6)	4.1(4)	339(16)	7.7(15)	0.50(17)
21	62.92(15)	1.476(3)	49(7)	0.42(11)	22(6)	0.45(18)	0.8(11)
22	68.68(8)	1.3656(15)	66(8)	0.98(13)	113(7)	1.7(3)	0.9(3)
23	71.83(3)	1.3131(5)	116(16)	0.32(6)	65(5)	0.56(12)	0.9(3)
24	73.45(5)	1.2882(7)	152(19)	0.57(8)	151(7)	0.99(17)	0.9(3)

No.	2θ, °	Decay(ηL/mL)	Decay(ηH/mH)	Size, Å	Phase Name	Chemical Formula
1	7.531(18)	1.2(4)	1.1(3)	229(41)	Unknown: 0 0 0	
2	10.6(3)	1.2(3)	1.55(12)	19.0(19)	Unknown: 0 0 0	
3	20.950(15)	0.3(6)	0.7(4)	230(31)	Unknown: 0 0 0	
4	23.01(2)	0.7(7)	0.0(11)	265(57)	Calcium Carbonate: 0 1 2	Ca (C O3)
5	24.867(15)	0.20(17)	0.41(12)	209(7)	Unknown: 0 0 0	
6	27.011(11)	0.64(12)	0.00(9)	227(6)	Unknown: 0 0 0	
7	29.326(15)	0.0(3)	0.00(19)	331(14)	Calcium Carbonate: 1 0 4	Ca (C O3)
8	32.760(11)	0.00(8)	0.00(19)	222(5)	Unknown: 0 0 0	
9	33.15(19)	0.00(8)	0.00(19)	140(15)	Unknown: 0 0 0	
10	39.381(16)	1.55(18)	0.9(3)	240(45)	Calcium Carbonate: 1 1 3	Ca (C O3)
11	42.67(2)	0.81(15)	0.35(7)	218(28)	Unknown: 0 0 0	
12	43.149(9)	0.81(15)	0.35(7)	717(131)	Calcium Carbonate: 2 0 2	Ca (C O3)
13	43.788(14)	0.81(15)	0.35(7)	228(7)	Unknown: 0 0 0	
14	47.42(2)	1.4(4)	1.5(4)	436(99)	Calcium Carbonate: 0 1 8	Ca (C O3)
15	48.452(10)	0.66(13)	0.84(10)	464(68)	Calcium Carbonate: 1 1 6	Ca (C O3)
16	49.037(19)	0.66(13)	0.84(10)	204(14)	Unknown: 0 0 0	
17	50.015(16)	0.66(13)	0.84(10)	220(8)	Unknown: 0 0 0	
18	55.81(4)	1.2(2)	1.4(2)	188(21)	Unknown: 0 0 0	
19	57.39(3)	0.3(8)	0.9(8)	530(125)	Calcium Carbonate: 1 2 2	Ca (C O3)
20	60.27(9)	0.7(3)	1.55(9)	23(2)	Calcium Carbonate: 2 1 4	Ca (C O3)
21	62.92(15)	0.0(15)	0.0(12)	232(60)	Calcium Carbonate: 1 2 5	Ca (C O3)
22	68.68(8)	1.2(3)	1.2(2)	102(14)	Calcium Carbonate: 2 1 7	Ca (C O3)
23	71.83(3)	1.2(3)	1.2(2)	319(57)	Unknown: 0 0 0	
24	73.45(5)	1.2(3)	1.2(2)	181(25)	Calcium Carbonate: 3 0 6	Ca (C O3)

No.	2θ, °	Card No	Norm. I.	Profile Type	Distributi...	Degree of Orientation
1	7.531(18)		12.29	Split pseudo-Voigt	-	-
2	10.6(3)		100.00	Split pseudo-Voigt	-	-
3	20.950(15)		6.53	Split pseudo-Voigt	-	-
4	23.01(2)	01-080-9776	2.97	Split pseudo-Voigt	-	-
5	24.867(15)		30.32	Split pseudo-Voigt	-	-
6	27.011(11)		49.41	Split pseudo-Voigt	-	-
7	29.326(15)	01-080-9776	15.87	Split pseudo-Voigt	-	-
8	32.760(11)		37.10	Split pseudo-Voigt	-	-
9	33.15(19)		7.68	Split pseudo-Voigt	-	-
10	39.381(16)	01-080-9776	11.63	Split pseudo-Voigt	-	-
11	42.67(2)		4.55	Split pseudo-Voigt	-	-
12	43.149(9)	01-080-9776	2.30	Split pseudo-Voigt	-	-
13	43.788(14)		32.45	Split pseudo-Voigt	-	-
14	47.42(2)	01-080-9776	5.80	Split pseudo-Voigt	-	-
15	48.452(10)	01-080-9776	4.33	Split pseudo-Voigt	-	-
16	49.037(19)		14.41	Split pseudo-Voigt	-	-
17	50.015(16)		31.68	Split pseudo-Voigt	-	-
18	55.81(4)		18.59	Split pseudo-Voigt	-	-
19	57.39(3)	01-080-9776	2.06	Split pseudo-Voigt	-	-
20	60.27(9)	01-080-9776	23.00	Split pseudo-Voigt	-	-
21	62.92(15)	01-080-9776	1.49	Split pseudo-Voigt	-	-
22	68.68(8)	01-080-9776	7.64	Split pseudo-Voigt	-	-
23	71.83(3)		4.39	Split pseudo-Voigt	-	-
24	73.45(5)	01-080-9776	10.22	Split pseudo-Voigt	-	-

No.	2θ, °	Ring Factor	β Cluster
1	7.531(18)	-	-
2	10.6(3)	-	-
3	20.950(15)	-	-
4	23.01(2)	-	-
5	24.867(15)	-	-
6	27.011(11)	-	-
7	29.326(15)	-	-
8	32.760(11)	-	-
9	33.15(19)	-	-
10	39.381(16)	-	-
11	42.67(2)	-	-
12	43.149(9)	-	-
13	43.788(14)	-	-
14	47.42(2)	-	-
15	48.452(10)	-	-
16	49.037(19)	-	-
17	50.015(16)	-	-
18	55.81(4)	-	-
19	57.39(3)	-	-
20	60.27(9)	-	-
21	62.92(15)	-	-
22	68.68(8)	-	-
23	71.83(3)	-	-
24	73.45(5)	-	-

Qualitative analysis results

Phase name	Formula	Figure of merit	Phase reg. detail	Space Group	DB Card Number
Calcium Carbonate	Ca (C O3)	1.469	S/M(PDF-2 Releas…	167 : R-3c:H	01-080-9776

Phase Data View

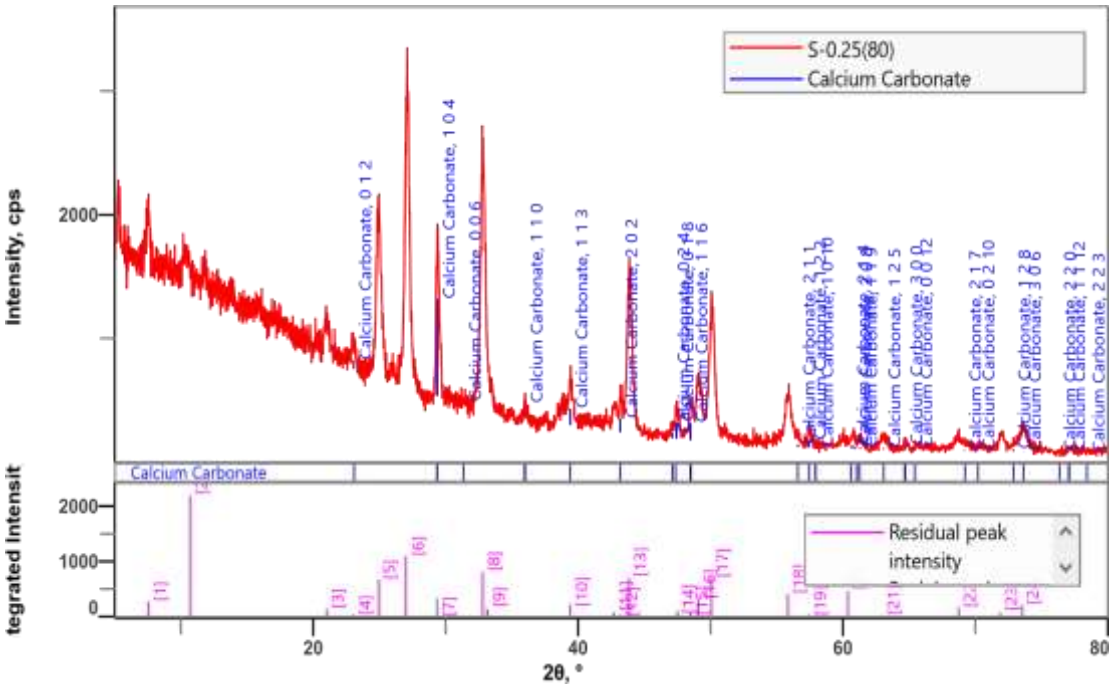

Lattice parameters

Phase name	a, Å	b, Å	c, Å	α, °	β, °	γ, °
Calcium Carbc	4.99039	4.99039	17.10886	90.000	90.000	120.000

d-I List
Calcium Carbonate

No.	2θ, °	d, Å	h k l	Norm. I.
1	23.03767	3.85746	0 1 2	9.40
2	29.35519	3.04009	1 0 4	100.00
3	31.34515	2.85148	0 0 6	1.90
4	35.96328	2.49519	1 1 0	13.90
5	39.38445	2.28597	1 1 3	17.00
6	43.14367	2.09509	2 0 2	14.30
7	47.07887	1.92873	0 2 4	6.20
8	47.39062	1.91677	0 1 8	17.50
9	48.43703	1.87777	1 1 6	17.60
10	56.55080	1.62609	2 1 1	2.70
11	57.38204	1.60450	1 2 2	7.60
12	57.92387	1.59077	1 0 10	0.90
13	60.63414	1.52599	2 1 4	4.30
14	60.89642	1.52004	2 0 8	1.80
15	61.24899	1.51214	1 1 9	2.00
16	63.00602	1.47413	1 2 5	1.60
17	64.64785	1.44060	3 0 0	4.80
18	65.40529	1.42574	0 0 12	2.60
19	69.10869	1.35810	2 1 7	0.80
20	70.09637	1.34136	0 2 10	1.30
21	72.79547	1.29813	1 2 8	2.10
22	73.60667	1.28582	3 0 6	0.40
23	73.60667	1.28582	0 3 6	0.00
24	76.25659	1.24760	2 2 0	0.90
25	76.96240	1.23791	1 1 12	1.40
26	78.39950	1.21877	2 2 3	0.10

Appendix D: Photo Gallery

Weight Measurement

Starch Adding at 100ml Distilled Water

Heating the Starch

Calcium Acetate Adding at Room Temperature

Heating of Calcium Acetate

Stirring After Adding Ammonium Carbonate

Centrifugation

Drying

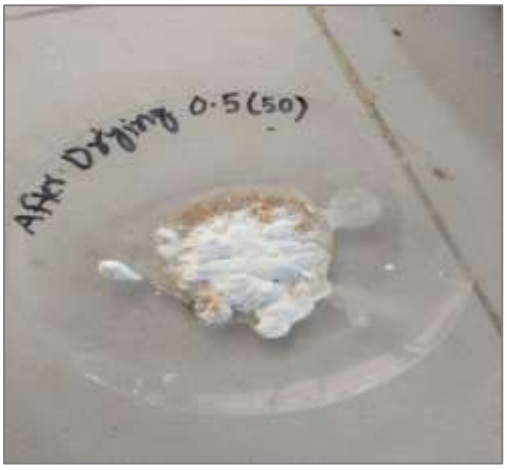

Condition After Drying

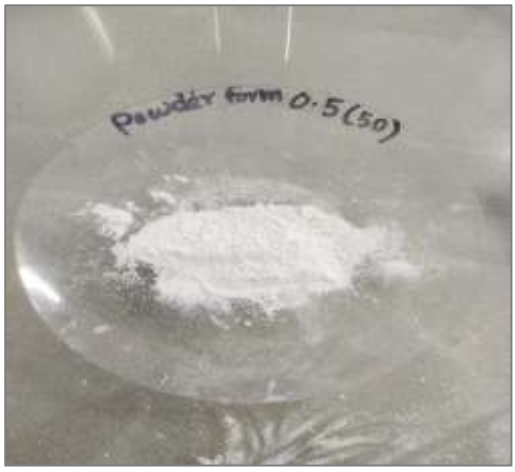

Final Powder Formation

Brief Biography

Sadia Tuz Zohra passed the Secondary School Certificate Examination in 2012 from Chakrashala Krishi High School, Patiya, Chattogram, Bangladesh and Advanced Secondary Certificate Examination in 2014 from Chattogram Biggan College, Chattogram, Bangladesh. She attained her B.Sc. (Honor's) in Food Science and Technology from the Faculty of Food Science and Technology at Chattogram Veterinary and Animal Sciences University, Chattogram, Bangladesh. She is enrolled at Food Chemistry and Quality Assurance master's program under the Department of Applied Chemistry and Chemical Technology, Chattogram Veterinary and Animal Sciences University (CVASU). She has an immense interest to work in perfecting the health status of people through proper guidance and suggestions and to produce mindfulness among people about food safety and nutrition.